Physics of Plasmas

Theory of edge localized mode suppression by static resonant magnetic perturbations in the DIII-D tokamak

Cite as: Phys. Plasmas **27**, 042506 (2020); https://doi.org/10.1063/5.0003117
Submitted: 31 January 2020 . Accepted: 13 March 2020 . Published Online: 02 April 2020

Richard Fitzpatrick

COLLECTIONS

This paper was selected as Featured

View Online Export Citation CrossMark

ARTICLES YOU MAY BE INTERESTED IN

A new explanation of the sawtooth phenomena in tokamaks
Physics of Plasmas **27**, 032509 (2020); https://doi.org/10.1063/1.5140968

Gyrokinetic particle simulations of interactions between energetic particles and magnetic islands induced by neoclassical tearing modes
Physics of Plasmas **27**, 032508 (2020); https://doi.org/10.1063/1.5126681

GTC simulation of linear stability of tearing mode and a model magnetic island stabilization by ECCD in toroidal plasma
Physics of Plasmas **27**, 042507 (2020); https://doi.org/10.1063/1.5111127

AIP Publishing

© 2020 Author(s).

Physics of Plasmas ARTICLE scitation.org/journal/php

Theory of edge localized mode suppression by static resonant magnetic perturbations in the DIII-D tokamak

Cite as: Phys. Plasmas **27**, 042506 (2020); doi: 10.1063/5.0003117
Submitted: 31 January 2020 · Accepted: 13 March 2020 ·
Published Online: 2 April 2020

View Online Export Citation CrossMark

Richard Fitzpatrick[a)]

AFFILIATIONS

Institute for Fusion Studies, Department of Physics, University of Texas at Austin, Austin, Texas 78712, USA

[a)]Author to whom correspondence should be addressed: rfitzp1632@gmail.com

ABSTRACT

According to a recent paper [Hu *et al.*, Phys. Plasmas **26**, 120702 (2019)], mode penetration at the top of the pedestal is a necessary and sufficient condition for the suppression of edge localized modes (ELMs) by a resonant magnetic perturbation (RMPs) in an H-mode tokamak discharge. This paper employs asymptotic matching theory to model a particular DIII-D discharge in which ELMs were suppressed by an externally generated, static, $n = 2$, RMP whose amplitude was modulated at a frequency of 1 Hz. It is demonstrated that the response of the plasma to the applied RMP, in the immediate vicinities of the rational (i.e., resonant) surfaces, is governed by *nonlinear*, rather than by linear, physics. This is the case because the magnetic island widths associated with driven reconnection exceed the linear layer widths, even in cases where driven reconnection is strongly suppressed by plasma rotation. The natural frequency at a given rational surface (i.e., the helical frequency at which the locally resonant component of the RMP would need to propagate in order to maximize driven reconnection) is found to be offset from the local $\mathbf{E} \times \mathbf{B}$ frame in the *ion* diamagnetic direction. The size of the offset is mostly determined by neoclassical poloidal rotation. Finally, the predictions of a fully nonlinear plasma response model are found to be broadly consistent with the DIII-D experimental data.

Published under license by AIP Publishing. https://doi.org/10.1063/5.0003117

I. INTRODUCTION

Tokamak discharges operating in high-confinement mode (H-mode)[1] exhibit intermittent bursts of heat and particle transport, emanating from the outer regions of the plasma, that are known as *type-I edge localized modes* (ELMs).[2] ELMs are fairly harmless in present-day tokamaks possessing carbon plasma-facing components. However, large ELMs can cause a problematic influx of tungsten ions into the plasma core in tokamaks possessing tungsten plasma-facing components.[3] Moreover, it is estimated that the heat load that ELMs will deliver to the tungsten plasma-facing components in a reactor-scale tokamak will be large enough to cause massive tungsten ion influx into the core, and that the erosion associated with this process will unacceptably limit the lifetimes of these components.[4] Consequently, the development of robust and effective methods for ELM control is a high priority for the international magnetic fusion program.

The most promising method for the control of ELMs is via the application of static *resonant magnetic perturbations* (RMPs). Complete RMP-induced ELM suppression was first demonstrated on the DIII-D tokamak.[5] Subsequently, either mitigation or complete suppression of ELMs has been demonstrated on the JET,[6] ASDEX-U,[7] KSTAR,[8] MAST,[9] and EAST[10] tokamaks.

ELMs are thought to be caused by peeling-ballooning instabilities, with intermediate toroidal mode numbers, that are driven by the strong pressure gradients and current density gradients characteristic of the edge region of an H-mode tokamak discharge,[11] which is known as the *pedestal* region. The initial observations of RMP-induced ELM suppression were interpreted as an indication that the magnetic field in the pedestal is rendered stochastic by the applied RMP, leading to greatly enhanced transport via thermal diffusion along magnetic field-lines.[5,12] This explanation was quickly abandoned because no significant reduction in the electron temperature gradient in the pedestal is observed during RMP-induced ELM suppression experiments, whereas a very significant reduction would be expected in the presence of stochastic fields. It is now generally accepted that response currents generated within the pedestal, as a consequence of plasma rotation, play a crucial role in the perturbed equilibrium in the presence of RMPs, and that these currents act to prevent the formation of RMP-driven magnetic island chains—a process known as *shielding*—and, thereby, significantly reduce the stochasticity of the magnetic field.[13]

This paper concentrates on a particular (but completely typical) DIII-D H-mode discharge (#158115[14]) in which ELMs were successfully suppressed by an externally applied $n = 2$ RMP. In this discharge,

Published under license by AIP Publishing

the relative phase of magnetic perturbations generated by two sets of external field coils is modulated sinusoidally at a frequency of 1 Hz, causing the amplitudes of the helical harmonics of the applied RMP that resonate in the pedestal region to modulate in a cycloidal manner at the same frequency. The application of the RMP is observed to generate two distinct plasma responses. The first response—which is known as the *density pump-out*—is characterized by a reduction in the pedestal density, accompanied by a much smaller reduction in the pedestal temperature, whose magnitude varies smoothly with the amplitude of the edge-resonant components of the RMP. The density pump-out is not observed to be associated with ELM suppression. The second response—which is known as *mode penetration*—occurs when the amplitude of the edge-resonant harmonics of the RMP exceeds a certain critical value, is associated with the sudden formation of a locked magnetic island chain at a rational surface that lies close to the top of the pedestal, and is accompanied by a sudden shift in the edge ion toroidal rotation. Mode penetration is observed to be strongly correlated with ELM suppression. If the amplitude of the edge-resonant harmonics of the RMP falls below a second, somewhat smaller, critical value, then the locked magnetic island chain is expelled from the plasma, and the edge ion toroidal rotation returns to its original value—this process is known as *mode unlocking*. Mode unlocking is invariably accompanied by the resumption of ELMs. Note that we can be fairly sure that mode penetration is associated with the formation of a locked magnetic island chain because when mode unlocking occurs the chain is sometimes observed to spin-up and decay away. (See, for example, Fig. 5 in Ref. 14.) The fact that mode penetration is a *necessary* condition for ELM suppression is a reasonable inference from existing DIII-D experimental data.[14] It is the hypothesis of this paper that mode penetration is also a *sufficient* condition. Incidentally, it is not difficult to understand why the formation of a locked island chain close to the top of the pedestal might give rise to ELM suppression. The flattening of the temperature and density profiles across the island region reduces the pressure gradient at the top of the pedestal, which is likely to move the plasma further from the peeling-ballooning stability threshold. Moreover, the formation of a locked island is likely to enhance any nonlinear interaction between the applied RMP and the peeling-ballooning mode (essentially by allowing the associated magnetic fields to phase lock to one another).[15,16]

A complete numerical simulation of DIII-D discharge #158115 would entail running a nonlinear extended (because the code would need to incorporate diamagnetic and neoclassical effects) full-magnetohyrodynamical (MHD) (because ELMs cannot be modeled using reduced-MHD) code in toroidal geometry (because ELMs cannot be modeled in cylindrical geometry) for approximately 10^8 Alfvén times (which corresponds to 1 s of experimental time). Unfortunately, this is completely impossible. (The most advanced, current-day, nonlinear, toroidal, extended-MHD codes are typically only capable of running for 10^4 Alfvén times.[15,16]) Hence, to make further progress, some sort of reduced model is required. If we accept that mode penetration is a sufficient condition for the achievement of ELM suppression, then the problem is greatly simplified, because we do not need to directly model ELMs, and, thus, we can perform a nonlinear reduced-MHD calculation in cylindrical geometry. This is precisely the approach taken in a recent paper by Hu *et al.*[17] In this paper, computer simulations—made using the cylindrical, multi-harmonic, five-field, nonlinear, initial-value code, TM1[18–20]—of DIII-D discharge #158115 find that the formation of RMP-driven magnetic island chains at the bottom and the top of the pedestal can account, in a quantitative fashion, for the observed density pump-out, as well as the mode-penetration-induced ELM suppression threshold.[17] The simulations also find that driven magnetic reconnection is strongly shielded in the middle of the pedestal. (Incidentally, the five fields in TM1 are the poloidal magnetic flux, the electron density, the perpendicular ion vorticity, the parallel ion velocity, and the electron temperature.) It should be noted that the simulations presented in Ref. 17 use the experimental density, temperature, safety-factor, and radial electric field profiles, apply an appropriately modulated $n = 2$ RMP with the experimental spectrum of resonant harmonics, and simulate the response of the plasma for the equivalent of 2.5 s of experimental time.

Generally speaking, a tokamak plasma exhibits two distinct types of response to an applied RMP. The first of these is the conventional *tearing response* due to magnetic islands driven at rational surfaces within the plasma. The second is the *kink response*[21,22] due to coupling to a non-resonant stable kink mode. The kink response causes the plasma to effectively amplify the applied RMP. Although the cylindrical TM1 code cannot directly determine the kink response of the plasma, the kink-induced amplification of the RMP can be correctly calculated using a linear toroidal ideal-MHD code such as the HINT[23] or IPEC[24] codes. The amplified RMP calculated by HINT or IPEC can then be used (as, indeed, it is used) as a boundary condition for the TM1 code.[17]

Unfortunately, even the reduced model of Ref. 17 requires many tens of hours of cpu time (corresponding to many days of actual time) to perform a complete simulation. The first aim of this paper is to employ standard asymptotic matching theory to further simplify the model in such a manner that a complete simulation can be performed in a matter of minutes in real time. The second, and equally important, aim is to gain a more exact understanding of the physical mechanism that underlies RMP-induced ELM suppression in the DIII-D tokamak. Two asymptotic matching theories are employed in this study. The first employs the cylindrical, single-harmonic, four-field, *linear*, resonant plasma response model of Refs. 25 and 26. The second employs the cylindrical, single-harmonic, four-field, *nonlinear*, resonant plasma response model of Refs. 27–29. (Note that, unlike the model used in Ref. 17, for the sake of simplicity, the models used in this paper do not evolve the electron temperature profile separately from the density profile. Hence, they are four-field, rather than five-field, models.)

II. PRELIMINARY ANALYSIS

A. Plasma equilibrium

Consider a large aspect-ratio, low-β, tokamak plasma whose equilibrium magnetic flux surfaces map out (almost) concentric circles in the poloidal plane. Such a plasma is well approximated as a periodic cylinder. Suppose that the minor radius of the plasma is a. Standard *right-handed* cylindrical coordinates (r, θ, z) are adopted. The system is assumed to be periodic in the z-direction, with periodicity length $2\pi R_0$, where $R_0 \gg a$ is the simulated plasma major radius. It is convenient to define the simulated toroidal angle $\phi = z/R_0$.

The equilibrium magnetic field is written as $\mathbf{B}(\mathbf{r}) = [0, B_\theta(r), B_\phi]$. The associated equilibrium plasma current density takes the form $\mathbf{j}(\mathbf{r}) = [0, 0, j_\phi(r)]$, where

Published under license by AIP Publishing

$$\mu_0 j_\phi(r) = \frac{1}{r}\frac{d(r B_\theta)}{dr}. \quad (1)$$

The safety factor

$$q(r) = \frac{r B_\phi}{R_0 B_\theta}, \quad (2)$$

parameterizes the helical pitches of equilibrium magnetic field-lines. In a conventional tokamak plasma, $|q(r)|$ is of order unity, and is a monotonically increasing function of r.

B. Plasma response

Consider the response of the plasma to a static RMP. Suppose that the RMP has $|m|$ periods in the poloidal direction, and $n > 0$ periods in the toroidal direction. (Note that m is positive if q is positive, and vice versa. It turns out that q is negative in DIII-D discharge #158115.) It is convenient to express the perturbed magnetic field and the perturbed plasma current density in terms of a magnetic flux-function, $\psi(r, \theta, \phi, t)$. Thus

$$\delta\mathbf{B} = \nabla\psi \times \mathbf{e}_z, \quad (3)$$

$$\mu_0\, \delta\mathbf{j} = -\nabla^2\psi\, \mathbf{e}_z, \quad (4)$$

where

$$\psi(r, \theta, \phi, t) = \hat{\psi}(r, t)\, \exp\left[\mathrm{i}\,(m\,\theta - n\,\phi)\right]. \quad (5)$$

This representation is valid provided that $|m|/n \gg a/R_0$.[30]

According to standard asymptotic matching theory, the response of the plasma to the applied RMP is governed by the equations of perturbed, marginally stable (i.e., $\partial/\partial t \equiv 0$), *ideal magnetohydrodynamics* (MHD) to an excellent approximation everywhere in the plasma, apart from a relatively narrow (in r) region in the vicinity of the rational surface, minor radius r_s, where $q(r_s) = m/n$.[30–32] This is essentially the case because the resistive term in the plasma Ohm's law is many orders of magnitude smaller than the other terms. Moreover, the scalar pressure gradient and the $\mathbf{j} \times \mathbf{B}$ terms in the plasma equation of motion are many orders of magnitude larger than the inertial, neoclassical viscous, or perpendicular viscous terms. However, the small terms become significant in the immediate vicinity of the rational surface because the radial scale length becomes of order the linear layer width, or the nonlinear island width, both of which are much less than the plasma minor radius. The region of the plasma, in the immediate vicinity of the rational surface, in which the equations of marginally stable ideal MHD break down, is termed the *inner region*. The remainder of the plasma (as well as the surrounding vacuum) is termed the *outer region*.

In the outer region, the perturbed poloidal magnetic flux, $\hat{\psi}_{\rm out}(r, t)$, satisfies the *cylindrical tearing mode equation*[30]

$$\frac{1}{r}\frac{\partial}{\partial r}\left(r\,\frac{\partial\hat{\psi}_{\rm out}}{\partial r}\right) - \frac{m^2}{r^2}\,\hat{\psi}_{\rm out} + \frac{\mu_0\, m\,(dj_\phi/dr)\,\hat{\psi}_{\rm out}}{B_\theta\,(m\,q - n)} = 0, \quad (6)$$

which is obtained by linearizing the marginally stable ideal MHD relation $\nabla \times (-\nabla p + \mathbf{j} \times \mathbf{B}) \simeq 0$, and combining the resulting equation with Eqs. (3)–(5).

It is convenient to write the solution to the previous equation in the form

$$\hat{\psi}_{\rm out}(r, t) = \Psi_s(t)\,\hat{\psi}_{\rm hom}(r) + \Psi_c(t)\,\hat{\psi}_{\rm inhom}(r), \quad (7)$$

where

$$\hat{\psi}_{\rm hom}(r) = \begin{cases} 0 & r = 0 \\ 1 & r = r_s \\ 0 & r = \infty \end{cases} \quad (8)$$

and

$$\hat{\psi}_{\rm inhom}(r) = \begin{cases} 0 & r = r_s \\ 1 & r = r_c \\ 0 & r = \infty, \end{cases} \quad (9)$$

with

$$\left[\frac{d\hat{\psi}_{\rm inhom}}{dr}\right]_{r_c-}^{r_c+} = -1. \quad (10)$$

Here, it is assumed that the applied RMP is driven by an external helical current $\delta\mathbf{j}(\mathbf{r}, t) = \mu_0^{-1}\,\Psi_c(t)\,r_c^{-1}\delta(r - r_c)\,\exp\left[\mathrm{i}\,(m\,\theta - n\,\phi)\right]$, where $r_c > a$. Note that $\hat{\psi}_{\rm hom}(r)$ and $\hat{\psi}_{\rm inhom}(r)$ are real continuous functions that have gradient discontinuities across the inner region.

Suppose that $\hat{\psi}_{\rm in}(r, t)$ is the perturbed poloidal magnetic flux in the inner region. Asymptotic matching between the inner and outer regions yields

$$\Delta_{\rm in}(t) = \Delta_{\rm out}(t), \quad (11)$$

where

$$\Delta_{\rm in/out}(t) = \left[r\,\frac{\partial\hat{\psi}_{\rm in/out}}{\partial r}\right]_{r_s-}^{r_s+}. \quad (12)$$

It follows from Eq. (7) that

$$\Delta_{\rm in}(t) = \Delta'\,r_s\,\Psi_s(t) + 2\,|m|\,\Psi_v(t), \quad (13)$$

where

$$\Delta' = \left[\frac{d\ln\hat{\psi}}{dr}\right]_{r_s-}^{r_s+}, \quad (14)$$

$$\Psi_v(t) = \frac{\Psi_c(t)}{2\,|m|}\left[r\,\frac{d\hat{\psi}_{\rm inhom}}{dr}\right]_{r_s-}^{r_s+}. \quad (15)$$

Here, $\Psi_v(t) = |\Psi_v|\,\mathrm{e}^{-\mathrm{i}\varphi_v}$ is the so-called *vacuum flux*, and is (approximately) the value of $\hat{\psi}(r, t)$ at radius r_s in the presence of the RMP, but in the absence of the plasma. Moreover, φ_v is the helical phase of the RMP, and is assumed to be constant in time. Furthermore, $\Psi_s(t) = |\Psi_s|\,\mathrm{e}^{-\mathrm{i}\varphi_s}$, which is the actual value of $\hat{\psi}(r, t)$ at radius r_s, is termed the *reconnected magnetic flux*. Here, $\varphi_s(t)$ is the helical phase of the reconnected flux. The parameter Δ' is the familiar *tearing stability index*.[31] According to standard tearing mode theory,[31,33] if $\Delta' > 0$ then the m/n tearing mode spontaneously reconnects magnetic flux at the rational surface to form a helical magnetic island chain. In the following, it is assumed that $\Delta' < 0$, so that the m/n tearing mode is intrinsically stable. In this situation, any magnetic reconnection that takes place at the rational surface is due solely to the RMP.

Published under license by AIP Publishing

C. Semi-collisional resonant response regime

In this paper, we shall examine two different response regimes in the inner region. The first of these is the so-called *semi-collisonal regime*.[26,34,35] This is a linear, two-fluid, low-collisionality regime for which[26,27]

$$\Delta_{\rm in}(t) = \frac{\delta_{\rm SC}}{r_s}\,\tau_R\left[\frac{d}{dt} + {\rm i}\,\omega(t)\right]\Psi_s(t). \tag{16}$$

Here

$$\delta_{\rm SC} = \pi\,\frac{|n\,\omega_{*e}|^{1/2}\,\tau_H}{(\rho_s/r_s)\,\tau_R^{1/2}}\,r_s, \tag{17}$$

is the linear layer width,[26] whereas

$$\tau_H = \frac{R_0}{|B_\phi|}\,\frac{\sqrt{\mu_0\,\rho(r_s)}}{n\,s}, \tag{18}$$

$$\tau_R = \mu_0\,r_s^2\,\sigma(r_s), \tag{19}$$

$$\omega_{*e} = \frac{(dp_e/dr)_{r_s}}{e\,n_e(r_s)\,R_0\,B_\theta(r_s)}, \tag{20}$$

$$\rho_s = \frac{\sqrt{m_i\,T_e(r_s)}}{e\,|B_\phi|}, \tag{21}$$

are the hydromagnetic timescale, resistive diffusion timescale, electron diamagnetic frequency, and ion sound radius, respectively, at the rational surface. Moreover, $s = (d\ln q/d\ln r)_{r=r_s}$ is the local magnetic shear, m_i is the ion mass, and e is the magnitude of the electron charge. Furthermore, $\sigma(r)$, $n_e(r)$, $\rho(r) \equiv m_i\,n_e(r)$, $T_e(r)$, $p_e(r) \equiv n_e(r)\,T_e(r)$ are the equilibrium plasma electrical conductivity, electron number density, mass density, electron temperature, and electron pressure profiles, respectively. Finally

$$\omega(t) = m\,\Omega_\theta(r_s,t) - n\,\Omega_\phi(r_s,t), \tag{22}$$

where $\Omega_\theta(r,t)$ and $\Omega_\phi(r,t)$ are the plasma poloidal and toroidal angular velocity profiles, respectively. (To be more exact, $\Omega_\theta(r,t)$ and $\Omega_\phi(r,t)$ are the poloidal and toroidal angular velocity profiles of an imaginary fluid that convects reconnected magnetic flux at rational surfaces. It is assumed that changes in these velocity profiles are mirrored by changes in the actual plasma velocity profiles. In the absence of an RMP, a magnetic island convected by the imaginary fluid propagates at its so-called natural frequency. The relationship between the natural frequency and the $\mathbf{E}\times\mathbf{B}$ frequency is specified in Sec. II F.) It is helpful to define the viscous diffusion timescale at the rational surface

$$\tau_V = \frac{r_s^2\,\rho(r_s)}{\mu(r_s)}, \tag{23}$$

where $\mu(r)$ is the equilibrium plasma (perpendicular) viscosity profile.

It should be noted that the analysis of Ref. 26, combined with the experimental data listed in Table I, leads to the conclusion that the appropriate cylindrical, four-field, linear, plasma response regime in the inner region is the so-called SCi (first semi-collisional) regime. (In particular, the dimensionless parameters c_β, D, P, and Q that control the plasma response, according to the analysis of Ref. 26, are calculated at the $-8/2$ and the $-11/2$ rational surfaces in the pedestal of DIII-D discharge #158115[14] in Table II. In the first case, the fact that $D>1$ implies that we should consult Fig. 3 in Ref. 26. According to this figure, the fact that $c_\beta\,D < Q < D$ and $P>1$ indicates that the appropriate response regime at the $-8/2$ surface is the SCi regime. In the second case, the fact that $c_\beta^{1/3} < D < 1$ implies that we should consult Fig. 2 in Ref. 26. According to this figure, the fact that $Q<D$ and $P > Q^3/D^6$ indicates that the appropriate response regime at the $-11/2$ surface is the SCi regime. The response and layer thickness in the SCi regime are listed in Table I of Ref. 26.) Equation (16) is a slightly simplified implementation of the response of the plasma in the vicinity of the rational surface in the SCi regime.

TABLE I. Measured and estimated physics parameters at two rational surfaces in the pedestal of DIII-D discharge #158115. (See Fig. 2 of Ref. 17.) m is the poloidal mode number, n is the toroidal mode number, B_ϕ is the toroidal magnetic field (T), R_0 is the major radius (m), a is the minor radius (m), n_e is the electron number density (10^{19} m^{-3}), T_e is the electron temperature (keV), T_i is the ion temperature (keV), $\eta_i = d\ln T_i/d\ln n_e$, $Z_{\rm eff}$ is the conventional measure of impurity content, $\chi_\perp$ is the perpendicular momentum diffusivity (m^2 s^{-1}), $\omega_E = E_r/(R_0\,B_\theta)$ is the $\mathbf{E}\times\mathbf{B}$ frequency (krad s^{-1}), $\omega_{*e} = (dp_e/dr)/(e\,n_e\,R_0\,B_\theta)$ is the electron diamagnetic frequency (krad s^{-1}), $\hat{r}_s$ is the rational surface radius normalized to the plasma minor radius, s is the magnetic shear, M_i is the majority ion mass number, and $\Delta \equiv -\Delta'\,r_s/(2\,m)$.

m	n	B_ϕ	R_0	a	n_e	T_e	T_i	η_i	$Z_{\rm eff}$
−8	2	−1.94	1.75	0.93	2.8	1.4	1.4	1.9	2.5
−11	2	−1.94	1.75	0.93	0.75	0.12	0.12	1.8	2.5

m	n	$\chi_\perp$	ω_E	ω_{*e}	$\hat{r}_s$	s	M_i	Δ
−8	2	1.0	−21.3	−21.5	0.853	2.3	2.0	1.0
−11	2	1.0	−9.8	−12.8	0.974	11.2	2.0	1.0

Incidentally, the experimental data listed in Table I are derived from the safety-factor, electron number density, electron temperature, and $\mathbf{E}\times\mathbf{B}$ frequency profiles shown in Ref. 17. The electron diamagnetic frequency, magnetic shear, and η_i values listed in the table are calculated directly from these profiles. The electron and ion temperature profiles are assumed to be the same. The values of the perpendicular momentum diffusivity are obtained from the TRANSP code.[36] The values of the effective ion charge number, $Z_{\rm eff}$, come from line emission spectroscopy.

Equations (13) and (16) can be combined to give the following linear evolution equation for the reconnected magnetic flux

$$\frac{\delta_{\rm SC}}{r_s}\,\tau_R\left[\frac{d}{dt} + {\rm i}\,\omega(t)\right]\Psi_s(t) = \Delta'\,r_s\,\Psi_s(t) + 2\,|m|\,\Psi_v(t). \tag{24}$$

TABLE II. Input parameters for the analytic, cylindrical, single-helicity, four-field, linear, resonant plasma response model of Ref. 26 at two rational surfaces in the pedestal of DIII-D discharge #158115. m is the poloidal mode number, n is the toroidal mode number, $c_\beta = \sqrt{\beta}$ (where β is the usual dimensionless measure of plasma pressure), $D = S^{1/3}\,\rho_s/r_s$ (where $S = \tau_R/\tau_H$), $P = \tau_R/\tau_V$, and $Q = S^{1/3}\,|\omega_0|\,\tau_H/2$, with $\omega_0 = -n\,(\omega_E + \omega_{*e})$.

m	n	c_β	D	P	Q
−8	2	6.48×10^{-2}	$1.54\times10^{+0}$	$7.16\times10^{+0}$	$1.27\times10^{+0}$
−11	2	9.81×10^{-3}	3.43×10^{-1}	4.63×10^{-1}	6.16×10^{-2}

Published under license by AIP Publishing

The previous equation is conveniently rewritten as an *island width evolution equation*[27]

$$\frac{\delta_{\rm SC}}{r_s}\,\tau_R\,\frac{d}{dt}\left(\frac{W}{r_s}\right)=\frac{1}{2}\,\frac{W}{r_s}\left[\Delta'\,r_s+2\,|m|\left(\frac{W_v}{W}\right)^2\cos\varphi\right], \tag{25}$$

and an *island phase evolution equation*

$$\frac{\delta_{\rm SC}}{r_s}\,\tau_R\left(\frac{d\varphi}{dt}-\omega\right)=-2\,|m|\left(\frac{W_v}{W}\right)^2\sin\varphi. \tag{26}$$

Here

$$W(t)=4\left(\frac{|\Psi_s|}{s\,r_s\,|B_\theta(r_s)|}\right)^{1/2} r_s, \tag{27}$$

is the full (radial) width of the magnetic island chain that forms at the rational surface. (Incidentally, it is assumed that $W\ll r_s$.) Moreover

$$W_v(t)=4\left(\frac{|\Psi_v|}{s\,r_s\,|B_\theta(r_s)|}\right)^{1/2} r_s, \tag{28}$$

is termed the vacuum island width. Finally

$$\varphi(t)=\varphi_s(t)-\varphi_v, \tag{29}$$

is the helical phase of the island chain relative to the RMP. Note that although Eqs. (25) and (26) are nonlinear in W and φ, they are entirely equivalent to the linear evolution equation (24). Incidentally, it is clear from Eq. (26) that in the presence of an RMP the reconnected magnetic flux at the rational surface can slip substantially with respect to the local plasma (i.e., $d\varphi/dt-\omega\neq 0$). However, this type of slippage is only possible in linear resonant response regimes. Finally, although Eqs. (25) and (26) appear to become singular in the limit $W\rightarrow 0$, this appearance is misleading. Indeed, if the equations are rewritten in terms of the real and imaginary parts of the reconnected flux, then they are perfectly well behaved in the limit $W\rightarrow 0$. [See Eqs. (77) and (78).]

The semi-collisional response regime holds in the inner region when $W<\delta_{\rm SC}$. That is, when the magnetic island width falls below the linear layer width.

D. Rutherford resonant response regime

The second response regime investigated in this paper is the so-called *Rutherford regime*. This is a nonlinear regime in which[33]

$$\mathrm{Re}\left(\frac{\Delta_{\rm in}}{\Psi_s}\right)=\mathcal{I}\,\tau_R\,\frac{d}{dt}\left(\frac{W}{r_s}\right), \tag{30}$$

where $\mathcal{I}=0.8227$, and[30]

$$\frac{d\varphi_s}{dt}-\omega=0. \tag{31}$$

According to the previous equation, which is known as the *no-slip constraint*, the island chain is forced to co-rotate (without slippage) with the aforementioned (see Secs. II E and II C) magnetic-flux-convecting imaginary fluid at the rational surface. Note that, unlike Eq. (16), the $\Delta_{\rm in}$ value specified in Eq. (30) is nonlinear in $|\Psi_s|$ (becasue $W\propto|\Psi_s|^{1/2}$). Equations (13) and (30) can be combined to give the *Rutherford island width evolution equation*[33,38–40]

$$\mathcal{I}\,\tau_R\,\frac{d}{dt}\left(\frac{W}{r_s}\right)=\Delta'\,r_s+2\,|m|\left(\frac{W_v}{W}\right)^2\cos\varphi. \tag{32}$$

Note that we are neglecting terms on the right-hand side of the previous equation that emanate from the perturbed bootstrap current and magnetic field line curvature. The neglect of the bootstrap and curvature terms is justified because they scale as $1/W$,[28] whereas the RMP term scales as $1/W^2$. Hence, the RMP term is dominant at the relatively small island widths at which mode penetration is triggered. Likewise, we are also neglecting any finite-island-width corrections to Δ' since these corrections are only important at relatively large island widths.

The Rutherford response regime holds in the inner region when $W>\delta_{\rm SC}$. That is, when the magnetic island width exceeds the linear layer width.

E. Plasma angular velocity evolution

It is easily demonstrated that zero net electromagnetic torque can be exerted on magnetic flux surfaces located in a region of the plasma that is governed by the equations of marginally stable, ideal-MHD.[30,41,42] Thus, to the extent that the plasma response away from the rational surface is governed by marginally stable, ideal-MHD (which it is to an excellent approximation) any significant electromagnetic torque exerted on the plasma by the RMP develops in the immediate vicinity of the rational surface, where ideal-MHD breaks down. The net poloidal and toroidal electromagnetic torques exerted in the vicinity of the rational surface by the RMP take the forms[30,37,43]

$$T_{\theta\rm EM}=-\frac{4\pi^2\,|m|\,m\,R_0}{\mu_0}\,|\Psi_v|\,|\Psi_s|\,\sin\varphi, \tag{33}$$

$$T_{\phi\rm EM}=\frac{4\pi^2\,|m|\,n\,R_0}{\mu_0}\,|\Psi_v|\,|\Psi_s|\,\sin\varphi, \tag{34}$$

respectively.

We can write

$$\Omega_\theta(r,t)=\Omega_{\theta0}(r)+\Delta\Omega_\theta(r,t), \tag{35}$$

$$\Omega_\phi(r,t)=\Omega_{\phi0}(r)+\Delta\Omega_\phi(r,t), \tag{36}$$

where $\Omega_{\theta0}(r)$ and $\Omega_{\phi0}(r)$ are the equilibrium poloidal and toroidal plasma angular velocity profiles, respectively, whereas $\Delta\Omega_\theta(r,t)$ and $\Delta\Omega_\phi(r,t)$ are the respective modifications to these profiles induced by the aforementioned electromagnetic torques. The modifications to the angular velocity profiles are governed by the poloidal and toroidal angular equations of motion of the plasma, which take the respective forms[30,44,45]

$$4\pi^2\,R_0\left[(1+2\,q^2)\,\rho\,r^3\,\frac{\partial\Delta\Omega_\theta}{\partial t}-\frac{\partial}{\partial r}\left(\mu\,r^3\,\frac{\partial\Delta\Omega_\theta}{\partial r}\right)+\rho\,r^3\,\frac{\Delta\Omega_\theta}{\tau_\theta}\right]=T_{\theta\rm EM}\,\delta(r-r_s), \tag{37}$$

$$4\pi^2\,R_0^3\left[\rho\,r\,\frac{\partial\Delta\Omega_\phi}{\partial t}-\frac{\partial}{\partial r}\left(\mu\,r\,\frac{\partial\Delta\Omega_\phi}{\partial r}\right)+\rho\,r\,\frac{\Delta\Omega_\phi}{\tau_\phi}\right]=T_{\phi\rm EM}\,\delta(r-r_s), \tag{38}$$

and are subject to the spatial boundary conditions[30]

Published under license by AIP Publishing

$$\frac{\partial \Delta\Omega_\theta(0,t)}{\partial r} = \frac{\partial \Delta\Omega_\phi(0,t)}{\partial r} = 0, \tag{39}$$

$$\Delta\Omega_\theta(a,t) = \Delta\Omega_\phi(a,t) = 0. \tag{40}$$

Here, $\tau_\theta(r)$ is the neoclassical poloidal flow-damping time profile,[46] and $\tau_\phi(r)$ is the neoclassical toroidal flow-damping time profile. The neoclassical toroidal flow-damping is assumed to be generated by nonresonant components of the applied RMP.[47,48] The factor $(1+2\,q^2)$ in Eq. (37) derives from the fact that incompressible poloidal flow has a poloidaly varying toroidal component that effectively increases the plasma mass being accelerated by the poloidal flow-damping force.[44] It turns out that, in the presence of strong poloidal and toroidal flow-damping, the modifications to the plasma poloidal and toroidal angular velocity profiles are localized in the vicinity of the rational surface.[48] Assuming that this is the case, it is a good approximation to replace q, ρ, μ, τ_θ, and τ_ϕ in Eqs. (37) and (38) by their values at the rational surface. We are, nevertheless, assuming that the localization width greatly exceeds the linear layer width (or the island width, in the nonlinear case). Note that we are neglecting the finite radial width of the resistive layer/magnetic island in Eqs. (37) and (38), which accounts for the presence of delta functions on the right-hand sides. This approximation is justified because the resistive layer/magnetic island width is generally very much smaller than the plasma minor radius.

Equations (22), (35), and (36) imply that

$$\omega(t) = \omega_0 + m\,\Delta\Omega_\theta(r_s,t) - n\,\Delta\Omega_\phi(r_s,t), \tag{41}$$

where

$$\omega_0 = m\,\Omega_{\theta 0}(r_s) - n\,\Omega_{\phi 0}(r_s), \tag{42}$$

is the so-called *natural frequency* of the m/n tearing mode. In other words, ω_0 is the helical phase velocity of a naturally unstable m/n tearing mode in the absence of the RMP.

F. Natural frequency

According to the cylindrical, single-helicity, four-field, *linear* analysis of Ref. 26, the appropriate natural frequency in the semi-collisional resonant response regime is

$$\omega_0 = -n\,(\omega_E + \omega_{*e}), \tag{43}$$

where $\omega_E = E_r(r_s)/[R_0\,B_\theta(r_s)]$ is the $\mathbf{E}\times\mathbf{B}$ frequency at the rational surface, and $E_r(r)$ is the equilibrium radial electric field profile.

According to the cylindrical, single-helicity, four-field, *nonlinear* analysis of Ref. 26, the appropriate natural frequency in the Rutherford resonant response regime is

$$\omega_0 = -n\,\omega_E - n\left(1 - \frac{\eta_i\,\lambda_{\theta i}}{1+\eta_i}\right)\omega_{*i}, \tag{44}$$

where

$$\omega_{*i} = -\frac{(dp_i/dr)_{r_s}}{e\,n_e(r_s)\,R_0\,B_\theta(r_s)}, \tag{45}$$

is the ion diamagnetic frequency at the rational surface, $\eta_i = (d\ln T_i/d\ln n_e)_{r=r_s}$, $T_i(r)$ is the equilibrium ion temperature profile, $p_i(r) = n_e(r)\,T_i(r)$ is the equilibrium ion pressure profile, and the dimensionless neoclassical parameter $\lambda_{\theta i}$ is specified in Appendix B.

III. QUASI-LINEAR RESPONSE MODEL

A. Introduction

The response model summarized in this section is termed "quasi-linear" because, whereas the plasma response model in the inner region is linear, the overall model is nonlinear due to the nonlinear nature of the electromagnetic torques.

B. Un-normalized quasi-linear response model

According to Secs. II C and II E, the complete quasi-linear response model takes the form

$$\frac{\delta_{\rm SC}}{r_s}\,\tau_R\,\frac{d}{dt}\left(\frac{W}{4\,r_s}\right) = \frac{1}{2}\left(\frac{W}{4\,r_s}\right)\left[\Delta'\,r_s + 2\,|m|\left(\frac{W_v}{W}\right)^2\cos\varphi\right], \tag{46}$$

$$\frac{\delta_{\rm SC}}{r_s}\,\tau_R\left(\frac{d\varphi}{dt} - \omega\right) = -2\,|m|\left(\frac{W_v}{W}\right)^2\sin\varphi, \tag{47}$$

$$\omega = \omega_0 + m\,\Delta\Omega_\theta(r_s,t) - n\,\Delta\Omega_\phi(r_s,t), \tag{48}$$

$$\left[(1+2\,q_s^2)\,\rho\,r^3\,\frac{\partial\Delta\Omega_\theta}{\partial t} - \frac{\partial}{\partial r}\left(\mu\,r^3\,\frac{\partial\Delta\Omega_\theta}{\partial r}\right) + \rho\,r^3\,\frac{\Delta\Omega_\theta}{\tau_\theta}\right] = -\frac{|m|\,m}{\mu_0}\left(\frac{W_v}{4\,r_s}\right)^2\left(\frac{W}{4\,r_s}\right)^2[s\,r_s\,B_\theta(r_s)]^2\,\sin\varphi\,\delta(r-r_s), \tag{49}$$

$$R_0^2\left[\rho\,r\,\frac{\partial\Delta\Omega_\phi}{\partial t} - \frac{\partial}{\partial r}\left(\mu\,r\,\frac{\partial\Delta\Omega_\phi}{\partial r}\right) + \rho\,r\,\frac{\Delta\Omega_\phi}{\tau_\phi}\right] = \frac{|m|\,n}{\mu_0}\left(\frac{W_v}{4\,r_s}\right)^2\left(\frac{W}{4\,r_s}\right)^2[s\,r_s\,B_\theta(r_s)]^2\,\sin\varphi\,\delta(r-r_s), \tag{50}$$

$$\frac{\partial\Delta\Omega_\theta(0,t)}{\partial r} = \frac{\partial\Delta\Omega_\phi(0,t)}{\partial r} = 0, \tag{51}$$

$$\Delta\Omega_\theta(a,t) = \Delta\Omega_\phi(a,t) = 0, \tag{52}$$

where $q_s = m/n$.

C. Normalized quasi-linear response model

It is helpful to define the typical *semi-collisional magnetic reconnection timescale*

$$\tau_{\rm SC} = \frac{\delta_{\rm SC}}{r_s}\,\frac{\tau_R}{2\,|m|}. \tag{53}$$

Let $\hat r = r/a$, $\hat t = t/\tau_{\rm SC}$, $\hat\omega_0 = \omega_0\,\tau_{\rm SC}$, $\hat\omega_\theta(\hat r,\hat t) = -m\,\Delta\Omega_\theta(r,t)\,\tau_{\rm SC}$, $\hat\omega_\phi(\hat r,\hat t) = n\,\Delta\Omega_\phi(r,t)\,\tau_{\rm SC}$, $\hat W = W/\delta_{\rm SC}$, and $\hat W_v = W_v/\delta_{\rm SC}$. The normalized quasi-linear response model reduces to

$$\frac{d\hat W}{d\hat t} = \frac{\hat W}{2}\left[-\hat\Delta' + \left(\frac{\hat W_v}{\hat W}\right)^2\cos\varphi\right], \tag{54}$$

$$\frac{d\varphi}{d\hat t} = \hat\omega - \left(\frac{\hat W_v}{\hat W}\right)^2\sin\varphi, \tag{55}$$

$$\hat\omega = \hat\omega_0 - \hat\omega_\theta(\hat r_s,\hat t) - \hat\omega_\phi(\hat r_s,\hat t), \tag{56}$$

$$(1+2\,q_s^2)\,\hat r^3\,\frac{\partial\hat\omega_\theta}{\partial\hat t} - \nu_\mu\,\frac{\partial}{\partial\hat r}\left(\hat r^3\,\frac{\partial\hat\omega_\theta}{\partial\hat r}\right) + \nu_\theta\,\hat r^3\,\hat\omega_\theta = \frac{\hat W_v^2\,\hat W^2}{\hat W_0^4}\,\sin\varphi\,\delta(\hat r - \hat r_s), \tag{57}$$

Published under license by AIP Publishing

$$\hat{r}\,\frac{\partial\hat{\omega}_\phi}{\partial\hat{t}}-\nu_\mu\,\frac{\partial}{\partial\hat{r}}\left(\hat{r}\,\frac{\partial\hat{\omega}_\phi}{\partial\hat{r}}\right)+\nu_\phi\,\hat{r}\,\hat{\omega}_\phi$$
$$=\left(\frac{\epsilon_a}{q_s}\right)^2\frac{\hat{W}_v^2\,\hat{W}^2}{\hat{W}_0^4}\,\sin\varphi\,\delta(\hat{r}-\hat{r}_s),\tag{58}$$

$$\frac{\partial\hat{\omega}_\theta(0,\hat{t})}{\partial\hat{r}}=\frac{\partial\hat{\omega}_\phi(0,\hat{t})}{\partial\hat{r}}=0,\tag{59}$$

$$\hat{\omega}_\theta(1,\hat{t})=\hat{\omega}_\phi(1,\hat{t})=0,\tag{60}$$

where $\hat{r}_s=r_s/a$, $\hat{\Delta}'=(-\Delta'\,r_s)/(2\,|m|)$, $\epsilon_a=a/R_0$, $\nu_\theta=\tau_{SC}/\tau_\theta$, $\nu_\phi=\tau_{SC}/\tau_\phi$, $\nu_\mu=(\tau_{SC}/\tau_V)\,(r_s/a)^2$, $\hat{W}_0=W_0/\delta_{SC}$, and

$$W_0=4\left(2\,\frac{\tau_H^2}{\tau_{SC}\,\tau_R}\,\frac{r_s}{\delta_{SC}}\right)^{1/4}a.\tag{61}$$

D. Solution of plasma angular equations of motion

We can solve Eqs. (57)–(60) by writing[49]

$$\hat{\omega}_\theta(\hat{r},\hat{t})=\sum_{n=1,N}a_n(\hat{t})\,\frac{y_n(\hat{r})}{y_n(\hat{r}_s)},\tag{62}$$

$$\hat{\omega}_\phi(\hat{r},\hat{t})=\sum_{n=1,N}b_n(\hat{t})\,\frac{z_n(\hat{r})}{z_n(\hat{r}_s)},\tag{63}$$

where

$$y_n(\hat{r})=\frac{J_1(j_{1,n}\,\hat{r})}{\hat{r}},\tag{64}$$

$$z_n(\hat{r})=J_0(j_{0,n}\,\hat{r}).\tag{65}$$

The solution is exact in the limit $N\rightarrow\infty$. Here, $J_m(z)$ is a standard Bessel function, and $j_{m,n}$ denotes the nth zero of the $J_m(z)$ Bessel function.[50] It is easily demonstrated that

$$\frac{d}{d\hat{r}}\left(\hat{r}^3\,\frac{dy_n}{d\hat{r}}\right)=-j_{1,n}^2\,\hat{r}^3\,y_n,\tag{66}$$

$$\frac{d}{d\hat{r}}\left(\hat{r}\,\frac{dz_n}{d\hat{r}}\right)=-j_{0,n}^2\,\hat{r}\,z_n,\tag{67}$$

and[51]

$$\int_0^1\hat{r}^3\,y_n(\hat{r})\,y_m(\hat{r})\,d\hat{r}=\frac{1}{2}\left[J_2(j_{1,n})\right]^2\delta_{nm},\tag{68}$$

$$\int_0^1\hat{r}\,z_n(\hat{r})\,z_m(\hat{r})\,d\hat{r}=\frac{1}{2}\left[J_1(j_{0,n})\right]^2\delta_{nm}.\tag{69}$$

Hence, we obtain

$$(1+2\,q_s^2)\,\frac{da_n}{d\hat{t}}+(\nu_\theta+\nu_\mu j_{1,n}^2)\,a_n=\alpha_n(\hat{r}_s)\,\frac{\hat{W}_v^2\,\hat{W}^2}{\hat{W}_0^4}\,\sin\varphi,\tag{70}$$

$$\frac{db_n}{d\hat{t}}+(\nu_\phi+\nu_\mu j_{0,n}^2)\,b_n=\epsilon\,\beta_n(\hat{r}_s)\,\frac{\hat{W}_v^2\,\hat{W}^2}{\hat{W}_0^4}\,\sin\varphi,\tag{71}$$

and

$$\alpha_n=\left[\frac{\sqrt{2}\,J_1(j_{1,n}\,\hat{r}_s)}{\hat{r}_s\,J_2(j_{1,n})}\right]^2,\tag{72}$$

$$\beta_n=\left[\frac{\sqrt{2}\,J_0(j_{0,n}\,\hat{r}_s)}{J_1(j_{0,n})}\right]^2,\tag{73}$$

$$\epsilon=\left(\frac{\epsilon_a}{q_s}\right)^2.\tag{74}$$

E. Final form of the normalized quasi-linear response model

If we define

$$X=\hat{W}^2\,\cos\varphi,\tag{75}$$

$$Y=\hat{W}^2\,\sin\varphi,\tag{76}$$

then, the normalized quasi-linear model reduces to the following closed set of equations

$$\frac{dX}{d\hat{t}}=-\hat{\omega}\,Y-\hat{\Delta}'\,X+b_f,\tag{77}$$

$$\frac{dY}{d\hat{t}}=\hat{\omega}\,X-\hat{\Delta}'\,Y,\tag{78}$$

$$(1+2\,q_s^2)\,\frac{da_n}{d\hat{t}}+(\nu_\theta+\nu_\mu j_{1,n}^2)\,a_n=\alpha_n(\hat{r}_s)\,L\,b_f\,Y,\tag{79}$$

$$\frac{db_n}{d\hat{t}}+(\nu_\phi+\nu_\mu j_{0,n}^2)\,b_n=\epsilon\,\beta_n(\hat{r}_s)\,L\,b_f\,Y,\tag{80}$$

$$\hat{\omega}=\hat{\omega}_0-\sum_{n=1,N}a_n-\sum_{n=1,N}b_n,\tag{81}$$

where $b_f=\hat{W}_v^2$, and $L=\hat{W}_0^{-4}$.

IV. NONLINEAR RESPONSE MODEL

A. Introduction

The response model summarized in this section is termed "nonlinear" because the plasma response model in the inner region is nonlinear in nature.

B. Un-normalized nonlinear response model

According to Secs. II D and II E, the complete nonlinear response model takes the form

$$\mathcal{I}\,\tau_R\,\frac{d}{dt}\left(\frac{W}{r_s}\right)=\Delta'\,r_s+2\,|m|\left(\frac{W_v}{W}\right)^2\cos\varphi,\tag{82}$$

$$\frac{d\varphi}{dt}=\omega,\tag{83}$$

plus Eqs. (48)–(52).

C. Normalized nonlinear response model

The normalized form of the nonlinear response model is

$$\mathcal{I}\,\frac{d\hat{W}}{d\hat{t}}=-\hat{\Delta}'+\left(\frac{\hat{W}_v}{\hat{W}}\right)^2\cos\varphi,\tag{84}$$

Published under license by AIP Publishing

$$\frac{d\varphi}{d\hat{t}} = \hat{\omega}, \tag{85}$$

plus Eqs. (56)–(60).

D. Final form of the normalized nonlinear response model

If we express the normalized nonlinear plasma response model in terms of the variables X and Y, which are defined in Eqs. (75) and (76), then we get

$$\frac{dX}{d\hat{t}} = -\hat{\omega}\, Y - f(X,Y)\,\hat{\Delta}'\, X + f(X,Y)\left(\frac{X^2}{X^2+Y^2}\right) b_f, \tag{86}$$

$$\frac{dY}{d\hat{t}} = \hat{\omega}\, X - f(X,Y)\,\hat{\Delta}'\, Y + f(X,Y)\left(\frac{X\,Y}{X^2+Y^2}\right) b_f, \tag{87}$$

plus Eqs. (79)–(81), where

$$f(X,Y) = \begin{cases} 2/\mathcal{I} & (X^2+Y^2)^{1/4} < 1 \\ 2/\left[\mathcal{I}\,(X^2+Y^2)^{1/4}\right] & (X^2+Y^2)^{1/4} \geq 1. \end{cases} \tag{88}$$

Here, a slight modification has been made to Eqs. (86) and (87) in the linear regime, $\hat{W} < 1$, (in which case they are not valid anyway) in order to render them non-singular at the origin of the X-Y plane.

V. RESULTS

A. Introduction

According to Ref. 17, the density pump-out in DIII-D discharge #158115 is due to mode penetration at the $m = -11/n = 2$ rational surface, which lies at the bottom of the pedestal. The formation of a magnetic island chain at the $-11/2$ surface leads to a local flattening of the plasma temperature and density profiles via parallel transport along magnetic field-lines. In order to flatten the profiles, the island width must exceed certain critical values that depend on the ratios of the relevant parallel and perpendicular diffusivities at the rational surface.[52] For the case of the electron temperature, making use of the analysis of Ref. 52, as well as the data in Table I, we estimate the critical width to be

$$W_{\mathrm{crit}T_e} \simeq \left(\frac{\chi_\perp}{v_e\, r_s}\,\frac{1}{\epsilon_s\, s\, n}\right)^{1/3} r_s \simeq 7.9\times 10^{-3}\ \mathrm{m}, \tag{89}$$

where $v_e = \sqrt{T_e/m_e}$, $\epsilon_s = r_s/R_0$, $\chi_\perp$ is the perpendicular diffusivity, and m_e the electron mass. For the case of the density, we estimate the critical width to be

$$W_{\mathrm{crit}n_e} \simeq \left(\frac{\chi_\perp}{v_i\, r_s}\,\frac{1}{\epsilon_s\, s\, n}\right)^{1/3} r_s \simeq 3.1\times 10^{-2}\ \mathrm{m}, \tag{90}$$

where $v_i = \sqrt{T_i/m_i}$. If both profiles are flattened across the island chain then, as a consequence of the fact that the equilibrium density gradient at the $-11/2$ surface greatly exceeds the temperature gradient (i.e., because $n_e/(T_i\,\eta_i) \simeq 3.5$ $[10^{19}\,\mathrm{m}^{-3}/(\mathrm{keV})]$; see Table I, as well as Ref. 17), the flattening naturally produces a much larger reduction in the pedestal density (measured in units of $10^{19}\,\mathrm{m}^{-3}$) than in the pedestal temperature (measured in units of keV).

According to Ref. 17, ELM suppression in DIII-D discharge #158115 is due to mode penetration at the $m = -8/n = 2$ rational surface, which lies at the top of the pedestal. The formation of a magnetic island chain at the $-8/2$ surface leads to a local flattening of the plasma temperature and density profiles. As before, the island width must exceed certain critical values to flatten the profiles. We estimate the critical width required to flatten the electron temperature profile to be [see Eq. (89) and Table I]

$$W_{\mathrm{crit}T_e} \simeq 8.5\times 10^{-3}\ \mathrm{m}, \tag{91}$$

whereas the critical width required to flatten the density profile is [see Eq. (90) and Table I]

$$W_{\mathrm{crit}n_e} \simeq 3.3\times 10^{-2}\ \mathrm{m}. \tag{92}$$

The flattening of the temperature and density profiles at the $-8/2$ rational surface is presumed to be sufficient to prevent the plasma in the pedestal from ever exceeding the peeling-ballooning stability threshold, which leads to ELM suppression.

B. Quasi-linear simulations

Table I shows measured and estimated physics parameters at the $m = -8/n = 2$ and $m = -11/n = 2$ rational surfaces in DIII-D discharge #158115. Incidentally, all experimental minor radii quoted in this paper are flux-surfaced-averaged minor radii, rather than minor radii on the outboard mid-plane. Making use of the analysis contained in the Appendixes, these parameters can be used to derive the input parameters for the quasi-linear model [i.e., Eqs. (77)–(81)] that are listed in Table III. Note that the dimensionless toroidal flow-damping rate has been set to zero (mostly because there are insufficient data to calculate its value). Note, further, that our knowledge of the edge current profile in DIII-D discharge #158115 is insufficient to allow us to calculate the parameter $\hat{\Delta}'$ directly. Fortunately, in the limit that $|m| \gg 1$ (which is the case here) it is a good approximation to give this parameter its "vacuum" value unity. [This is equivalent to assuming that the term involving m^2/r^2 dominates the term involving dj_ϕ/dr in Eq. (6).] In DIII-D discharge #158115, the relative phase of

TABLE III. Input parameters for the quasi-linear response model at two rational surfaces in the pedestal of DIII-D discharge #158115. m is the poloidal mode number, n is the toroidal mode number, $\hat{r}_s$ is the rational surface radius normalized to the plasma minor radius, $\epsilon \equiv (\epsilon_a/q_s)^2$, ν_θ is the dimensionless poloidal flow damping parameter, ν_ϕ is the dimensionless toroidal flow-damping parameter, ν_μ is the dimensionless perpendicular viscosity parameter, L is the dimensionless locking parameter, and $\hat{\omega}_0$ is the normalized natural frequency. The latter quantity is calculated assuming that $\omega_0 = -n\,(\omega_E + \omega_{*e})$.

m	n	$\hat{r}_s$	ϵ	ν_θ	ν_ϕ	ν_μ	L	$\hat{\omega}_0$
−8	2	0.853	1.77×10^{-2}	$4.35\times10^{+2}$	0.0	2.16×10^{-3}	9.41×10^{-3}	$1.60\times10^{+2}$
−11	2	0.974	9.34×10^{-3}	$6.50\times10^{+1}$	0.0	1.32×10^{-4}	1.60×10^{-2}	$5.16\times10^{+0}$

Published under license by AIP Publishing

RMPs generated by two sets of external field coils is modulated sinusoidally at a frequency of 1 Hz. This causes the amplitudes of the resonant harmonics of the applied RMP to be modulated in a cycloidal manner at the same frequency.

Figure 1 shows a quasi-linear simulation of the response of the plasma at the $-8/2$ rational surface in DIII-D discharge #158115 to an RMP whose magnitude is switched on at $t=0$, and then modulated cycloidally at a frequency of 1 Hz. All simulations in this paper are performed with 200 velocity harmonics [i.e., $N=200$ in Eq. (81)]. The simulation data presented in Fig. 1 are qualitatively similar to the experimental data shown in Ref. 17, as well as the TM1 simulation data displayed in Fig. 2 of the same paper. In particular, if the amplitude of the applied RMP rises above a certain threshold value, then there is a bifurcation from a shielded solution characterized by $\hat{W} \ll \sqrt{b_f}$ to an unshielded solution characterized by $\hat{W} \sim \sqrt{b_f}$. This bifurcation, which is known as *mode penetration*, is accompanied by a sudden reduction in the natural frequency to zero, as well as sudden shifts in the plasma poloidal and toroidal rotation at the rational surface. Figure 2 shows the mode penetration process in more detail. Furthermore, referring again to Fig. 1, if the amplitude of the applied RMP falls below a second smaller threshold value, then there is a bifurcation from an unshielded solution to a shielded solution. This bifurcation, which is known as *mode unlocking*, is accompanied by the recovery of the natural frequency to its unperturbed value, as well as sudden shifts in the plasma poloidal and toroidal rotation at the

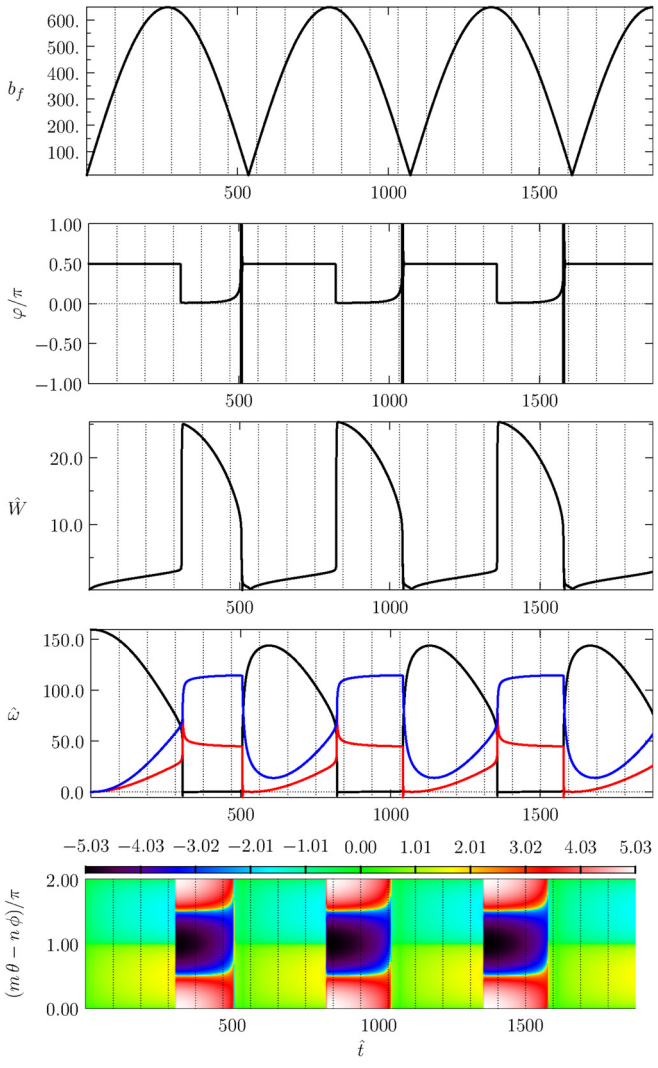

FIG. 1. Quasi-linear simulation of the plasma response to an applied RMP at the $m=-8/n=2$ rational surface in DIII-D discharge #158115. The top panel shows the applied RMP. The second panel shows the helical phase of the reconnected magnetic flux. The third panel shows the RMP-induced magnetic island width (normalized to δ_{SC}). The fourth panel shows the RMP-modified natural frequency, $\hat{\omega}$ (black curve), the RMP-induced shift in the plasma poloidal angular velocity, $\hat{\omega}_\theta$ (red curve), and the RMP-induced shift in the plasma toroidal angular velocity, $\hat{\omega}_\phi$ (blue curve). The previous three quantities are all normalized to $1/\tau_{SC}$. The bottom panel shows simulated Mirnov data. To be more exact, it shows contours of $\hat{W}^2 \cos[(m\theta - n\phi - \varphi)]$. $\hat{t}$ is time normalized to τ_{SC}.

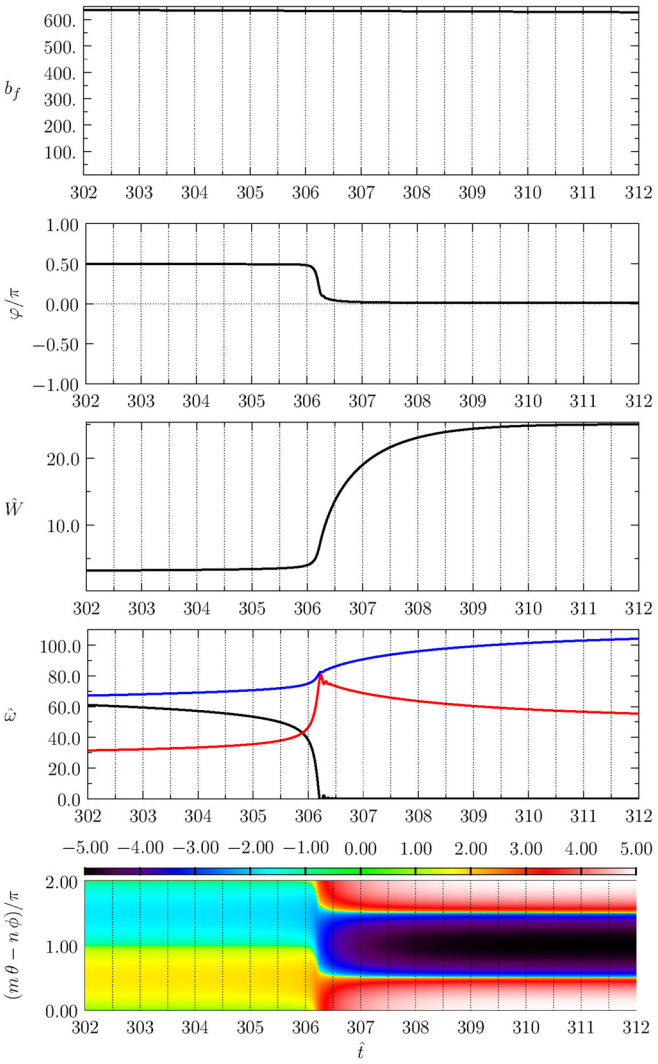

FIG. 2. Details of Fig. 1 showing mode penetration. See Fig. 1 caption.

Published under license by AIP Publishing

rational surface. Figure 3 shows the mode unlocking process in more detail. Note that, immediately after unlocking, the magnetic island chain at the rational surface spins-up and decays, before eventually re-locking to the RMP in a fixed helical phase relation. The lowest panels in Figs. 1–3 (as well as in Figs. 4–8) represent attempts to reproduce the type of experimental magnetic pickup coil array data epitomized by panels (b)–(e) in Fig. 2 of Ref. 17.

As is apparent from Fig. 1, mode penetration is triggered as soon as the natural frequency has been reduced to approximately one half of its unperturbed value.[30] Moreover, about one third of the reduction in the natural frequency associated with mode penetration is due to a shift in the local plasma poloidal rotation, whereas two thirds is due to a shift in the local toroidal rotation. In the absence of neoclassical poloidal flow-damping, only about 2% (i.e., a fraction ϵ—see Table III) of the change in the natural frequency would be due to a shift in local plasma toroidal rotation. The large increase in the fraction of the

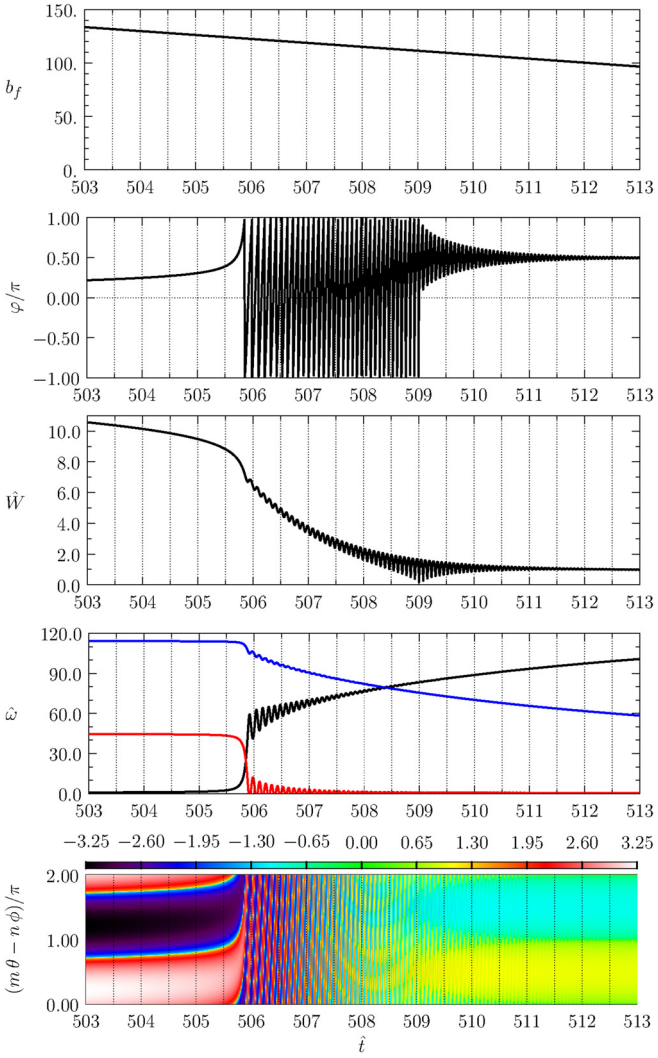

FIG. 3. Details of Fig. 1 showing mode unlocking. See Fig. 1 caption.

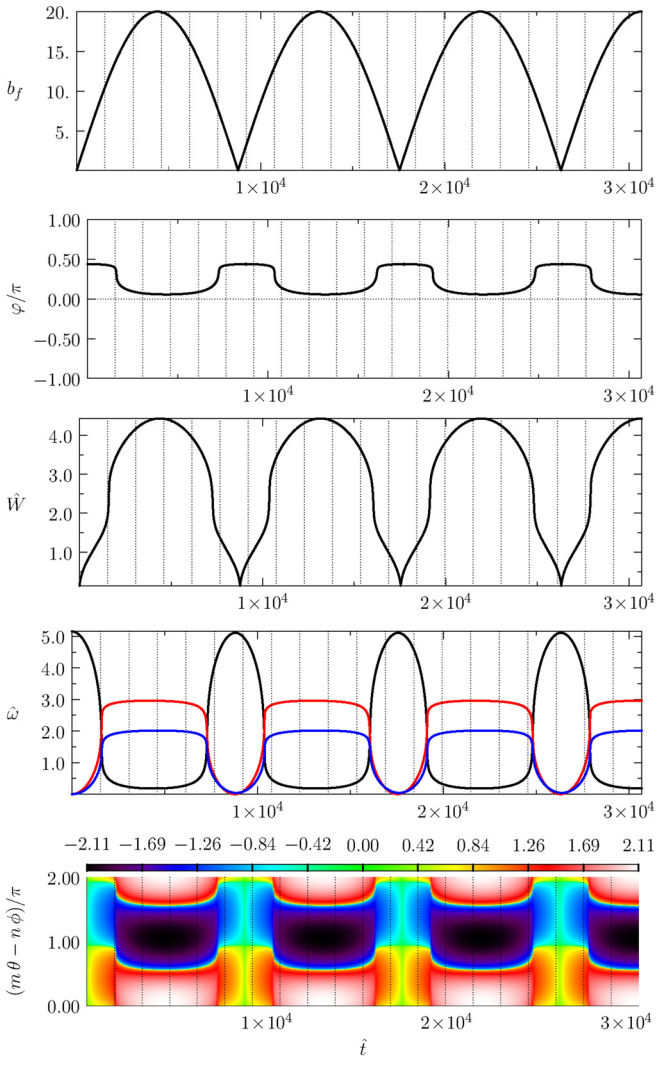

FIG. 4. Quasi-linear simulation of plasma response to an applied RMP at the $m = -11/n = 2$ rational surface in DIII-D discharge #158115. See Fig. 1 caption.

overall frequency change due to toroidal velocity shifts, in the presence of neoclassical poloidal flow-damping, is a consequence of the fact that a substantial fraction of the charged particles in the DIII-D pedestal are trapped in banana orbits, and cannot, therefore, freely rotate in the poloidal direction. Hence, neoclassical poloidal flow-damping is comparatively strong in the pedestal region of the DIII-D tokamak (compared to that in the plasma core). (The same is likely to be true in the pedestal regions of all relatively large, conventional aspect-ratio tokamaks.) The mode-penetration-induced shift in the plasma toroidal rotation shown in Fig. 1 corresponds to a toroidal velocity shift in the co-current direction of about 30 km/s (see Table IV), which is in agreement with experimental observations.[17] The mode-penetration-induced shift in the plasma poloidal rotation shown in Fig. 1 corresponds to a poloidal velocity shift in the ion diamagnetic direction of only about 2 km/s. Furthermore, we would expect the latter velocity

Published under license by AIP Publishing

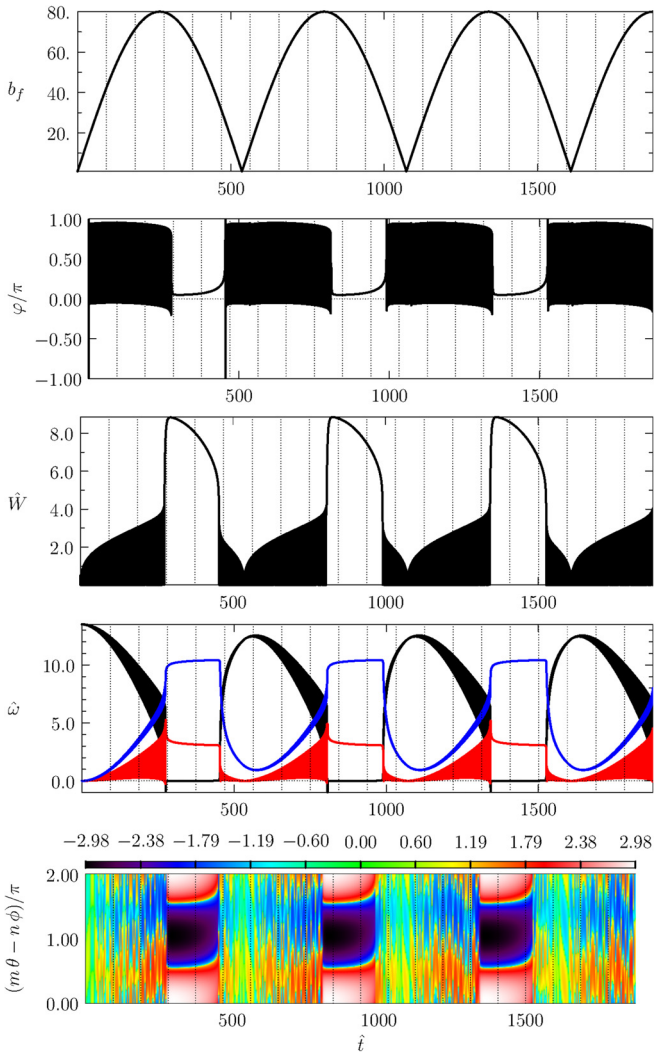

FIG. 5. Nonlinear simulation of plasma response to an applied RMP at the $m = -8/n = 2$ rational surface in DIII-D discharge #158115. See Fig. 1 caption.

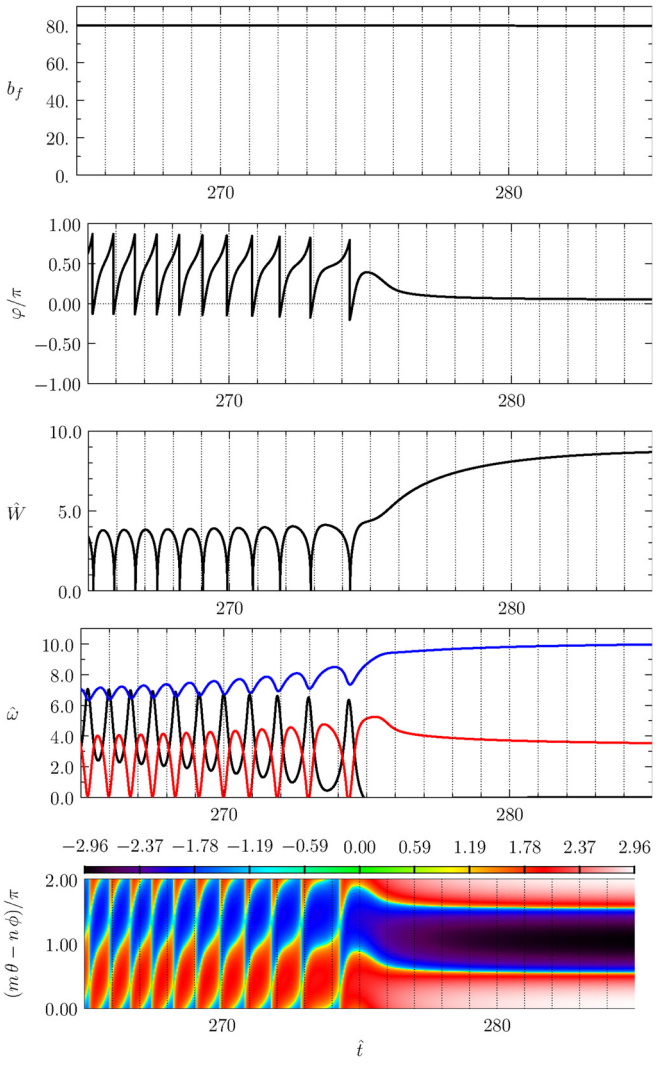

FIG. 6. Details of Fig. 5 showing mode penetration. See Fig. 1 caption.

shift to be strongly localized in the vicinity of the rational surface.[48] Hence, it is not surprising that the poloidal velocity shift is not observed experimentally.[53]

According to Figs. 2 and 3, the sudden collapse/recovery of the natural frequency associated with mode penetration/mode unlocking takes place on a timescale of about a millisecond (see Table IV), and is accompanied by a sudden shift in the local plasma poloidal rotation that takes place on the same timescale. The mode penetration/mode unlocking-induced shift in the local plasma toroidal rotation takes place on a significantly longer timescale (at least, 10 ms).

There is one major difference between the simulation data shown in Fig. 1 and the experimental and TM1 simulation data shown in Ref. 17. According to Fig. 1, mode penetration at the $-8/2$ rational surface in DIII-D discharge #158115 occurs when b_f exceeds the critical value 649, which corresponds to a vacuum radial field at the $-8/2$ surface of $b_v = 45$ G. (See Table IV.) However, the penetration threshold inferred from experimental data is more like $b_v = 6$ gauss.[17] This discrepancy is probably related to the fact that, according to Figs. 1 and 2, mode penetration at the $-8/2$ rational surface in DIII-D discharge #158115 occurs when $W \sim 4\,\delta_{SC}$, in other words, when the magnetic island width exceeds the linear layer width. Given that the quasi-linear model is only valid when $W < \delta_{SC}$, we conclude that mode penetration at the $-8/2$ rational surface in DIII-D discharge #158115 is actually governed by the nonlinear model. This particular conclusion is not consistent with the TM1 simulations described in Ref. 17, according to which mode penetration at the $-8/2$ rational surface seems to be governed by linear physics in the inner region (because of the absence of island pulsations in the TM1 simulations—see Sec. V C). One possible explanation for this disagreement is that plasma perpendicular viscosity is artificially increased by a large factor in TM1 simulations, in order to mimic the effect of strong neoclassical poloidal flow-damping, but such an increase may also artificially increase the linear

Published under license by AIP Publishing

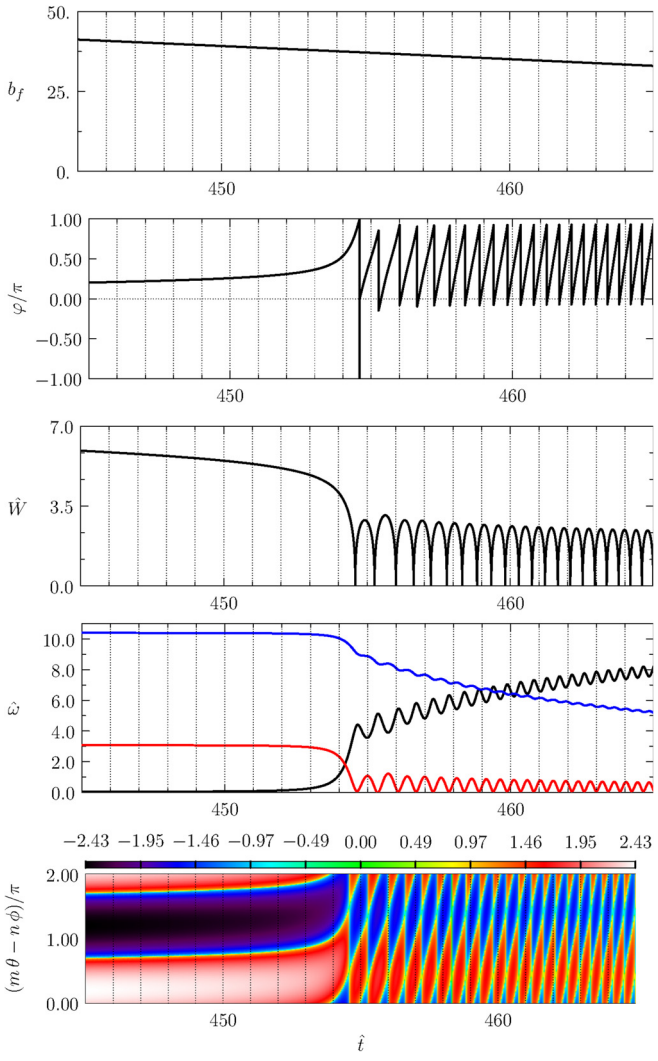

FIG. 7. Details of Fig. 5 showing mode unlocking. See Fig. 1 caption.

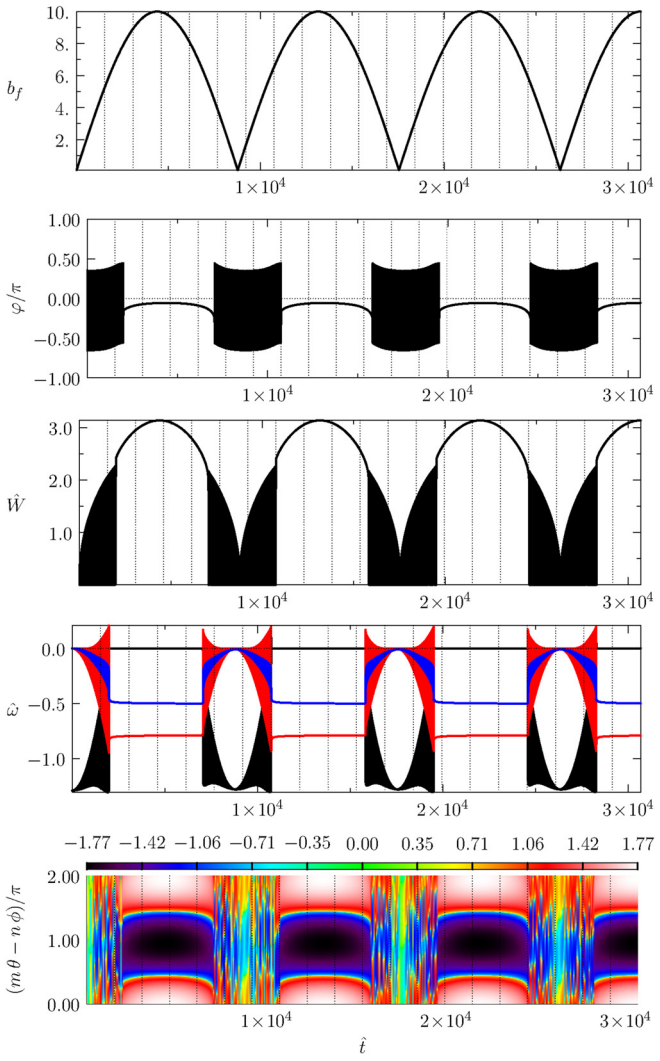

FIG. 8. Nonlinear simulation of plasma response to an applied RMP at the $m = -11/n = 2$ rational surface in DIII-D discharge #158115. See Fig. 1 caption.

layer width. Note, from Table IV, that the semi-collisional layer width at the $-8/2$ rational surface is only 4 mm, which is similar to the ion sound radius. On the other hand, the critical island width above which mode penetration is triggered is about 1.6 cm. Incidentally, after mode penetration has occurred, the $-8/2$ island width rises well above the values required to locally flatten the temperature and density profiles. (See Sec. V A.)

Figure 4 shows a quasi-linear simulation of the response of the plasma at the $-11/2$ rational surface in DIII-D discharge #158115 to an RMP whose magnitude is switched on at $t = 0$, and then modulated

TABLE IV. Important physical parameters at two rational surfaces in the pedestal of DIII-D discharge #158115. m is the poloidal mode number, n is the toroidal mode number, ν_{*e} is the dimensionless electron collisionality parameter, ν_{*i} is the dimensionless ion collisionality parameter, τ_{SC} is the semi-collisional reconnection timescale (s), δ_{SC} is the semi-collisional layer width (m), ρ_s is the ion sound radius (m), and b_f/b_v is the ratio of the normalized radial magnetic field to the vacuum radial magnetic field at the rational surface.

m	n	ν_{*e}	ν_{*i}	τ_{SC}	δ_{SC}	ρ_s	b_f/b_v
-8	2	9.26×10^{-2}	2.97×10^{-2}	1.86×10^{-3}	4.14×10^{-3}	2.79×10^{-3}	$1.45 \times 10^{+1}$
-11	2	$3.80 \times 10^{+0}$	$1.22 \times 10^{+0}$	1.14×10^{-4}	5.75×10^{-3}	8.16×10^{-4}	$1.77 \times 10^{+0}$

Published under license by AIP Publishing

cycloidally at a frequency of 1 Hz. The simulation data presented in Fig. 4 are qualitatively similar to the TM1 simulation data shown in Fig. 2 of Ref. 17. In particular, it is clear from Fig. 4 that there is insufficient plasma rotation at the −11/2 rational surface to enable the effective shielding of driven magnetic reconnection. In other words, $\hat{W} \sim \sqrt{b_f}$ at all times. This is the case because the plasma at the −11/2 surface is too cold and resistive for the levels of plasma rotation present at the edge of the pedestal to generate strong shielding. The peak −11/2 island width is sufficiently large to locally flatten the temperature and density profiles. (See Sec. V A.) Note, however, that $W > \delta_{SC}$, which implies that driven reconnection at the −11/2 rational surface in DIII-D discharge #158115 is actually governed by the nonlinear model.

C. Nonlinear simulations

Making use of the analysis contained in the Appendixes, the experimental data given in Table I can be used to derive the input parameters for the nonlinear model [i.e., Eqs. (86)–(88)] that are listed in Table V. Note that the dimensionless toroidal flow-damping rate has again been set to zero.

Figure 5 shows a fully nonlinear simulation of the response of the plasma at the −8/2 rational surface in DIII-D discharge #158115 to an RMP whose magnitude is switched on at $t = 0$, and then modulated cycloidally at a frequency of 1 Hz. The simulation data presented in Fig. 5 are qualitatively similar to the experimental data shown in Ref. 17. As before, if the amplitude of the applied RMP rises above a certain threshold value, then mode penetration occurs. In other words, there is bifurcation from a shielded to an unshielded solution, accompanied by a sudden reduction in the natural frequency to zero, as well as sudden shifts in the plasma toroidal and poloidal rotation at the rational surface. Figure 6 shows the mode penetration process in more detail. Furthermore, again referring to Fig. 5, if the amplitude of the applied RMP falls below a second smaller threshold value, then mode unlocking occurs. In other words, there is a bifurcation from an unshielded solution to a shielded solution, accompanied by the recovery of the natural frequency to its unperturbed value, as well as sudden shifts in the plasma toroidal and poloidal rotation at the rational surface. Figure 7 shows the mode unlocking process in more detail. As in the quasi-linear case, mode penetration is triggered when the natural frequency has been reduced to about half of its original value. Moreover, about two thirds of the change in the natural frequency associated with mode penetration/mode unlocking is due to a shift in the local toroidal plasma rotation, and about one third to a shift in the local poloidal plasma rotation.

The main difference between the nonlinear simulations discussed in this section and the quasi-linear simulations discussed in Sec. V B lies in the nature of the shielded solution. In the quasi-linear simulations, the shielded solution consists of a narrow magnetic island chain that has a fixed helical phase shift of about $+\pi/2$ with respect to the locally resonant component of the RMP. On the other hand, in the nonlinear simulations, the shielded solution consists of a narrow island chain whose helical phase continually increases in time, and whose width periodically falls to zero, at which times its helical phase jumps by $-\pi$ radians. This type of pulsating island solution was first predicted in Ref. 37, is discussed in detail in Refs. 27–29, and has been observed experimentally (see Fig. 29 in Ref. 54). Note, from Figs. 5 and 6, that the width of the pulsating island chain exceeds the linear layer width (i.e., $\hat{W} > 1$) during most of its cycle, which justifies the nonlinear response model employed in the inner region.

Figure 5 implies that mode penetration at the −8/2 rational surface in DIII-D discharge #158115 occurs when b_f exceeds the critical value 80, which corresponds to a vacuum radial field at the −8/2 surface of $b_v = 5.5$ G (see Table IV). This estimate for the penetration threshold is close to the experimentally inferred value of 6 G.[17]

According to Sec. II F, the natural frequency in the quasi-linear model is

$$\omega_0 = -n\,\omega_{\perp e}, \tag{93}$$

where $\omega_{\perp e} = \omega_E + \omega_{*e}$. On the other hand, the natural frequency in the nonlinear model is

$$\omega_0 = -n\,\omega_E - n\left(1 - \frac{\eta_i\,\lambda_{\theta i}}{1+\eta_i}\right)\omega_{*i}. \tag{94}$$

For the case of the −8/2 rational surface in DIII-D discharge #158115, $\eta_i = 1.9$ and $\lambda_{\theta i} = 0.272$, which implies that

$$\omega_0 = -n(\omega_E + 0.82\,\omega_{*i}), \tag{95}$$

in the nonlinear model. The fact that the natural rotation of a nonlinear magnetic island chain is offset in the ion diamagnetic direction, rather than the electron diamagnetic direction, relative to the local $\mathbf{E}\times\mathbf{B}$ frame, leads to a much smaller prediction for the natural frequency in the nonlinear model relative to that in the quasi-linear model. This is the main reason why the predicted penetration threshold for the nonlinear model is so much smaller than that for the quasi-linear model. According to the quasi-linear model, we would expect mode penetration at the −8/2 surface to be triggered when $\omega_{\perp e}$ passes through zero. Moreover, once mode penetration has occurred, and the natural frequency becomes zero, we would expect $\omega_{\perp e}$ to be pinned to zero at the rational surface. On the other hand, according to the nonlinear model, we would expect mode penetration at the −8/2 surface to be triggered when some frequency offset from the $\mathbf{E}\times\mathbf{B}$ frequency in the ion diamagnetic direction passes through zero. Moreover, once

TABLE V. Input parameters for the nonlinear response model at two rational surfaces in the pedestal of DIII-D discharge #158115. m is the poloidal mode number, n is the toroidal mode number, $\hat{r}_s$ is the rational surface radius normalized to the plasma minor radius, $\epsilon \equiv (\epsilon_a/q_s)^2$, ν_θ is the dimensionless poloidal flow damping parameter, ν_ϕ is the dimensionless toroidal flow-damping parameter, ν_μ is the dimensionless perpendicular viscosity parameter, L is the dimensionless locking parameter, and $\hat{\omega}_0$ is the normalized natural frequency. The latter quantity is calculated assuming that ω_0 is given by Eqs. (B20)–(B22).

m	n	$\hat{r}_s$	ϵ	ν_θ	ν_ϕ	ν_μ	L	$\hat{\omega}_0$
−8	2	0.853	1.77×10^{-2}	$4.35\times10^{+2}$	0.0	2.16×10^{-3}	9.41×10^{-3}	$6.97\times10^{+1}$
−11	2	0.974	9.34×10^{-3}	$6.50\times10^{+1}$	0.0	1.32×10^{-4}	1.60×10^{-2}	-9.72×10^{-1}

Published under license by AIP Publishing

mode penetration has occurred, and the natural frequency becomes zero, we would expect the offset frequency to be pinned to zero at the rational surface. In fact, experimental RMP-induced ELM suppression data from the DIII-D tokamak are not consistent with $\omega_{\perp e}$ being the trigger frequency,[55] but rather some frequency offset from $\omega_{\perp e}$ in the ion diamagnetic direction, which constitutes strong evidence that mode penetration at the top of the pedestal in DIII-D RMP-induced ELM suppression experiments is not governed by the quasi-linear model. Incidentally, there is clear experimental evidence that the helical phase velocity of a naturally unstable, nonlinear, magnetic island chain is offset in the ion diamagnetic direction relative to the local $\mathbf{E}\times\mathbf{B}$ frame.[56,57]

Figure 8 shows a nonlinear simulation of the response of the plasma at the $-11/2$ rational surface in DIII-D discharge #158115 to an RMP whose magnitude is switched on at $t=0$, and then modulated cycloidally at a frequency of 1 Hz. The simulation data presented in Fig. 8 are qualitatively similar the TM1 simulation data shown in Fig. 2 of Ref. 17. In particular, it is clear from Fig. 8 that there is not enough plasma rotation at the $-11/2$ rational surface to enable the effective shielding of driven magnetic reconnection. In other words, $\hat{W}\sim\sqrt{b_f}\equiv\hat{W}_f$ at all times. As before, this is the case because the plasma at the $-11/2$ surface is too cold and resistive for the levels of plasma rotation present at the edge of the pedestal to generate strong shielding. Note, however, that $W>\delta_{SC}$, which confirms that driven reconnection at the $-11/2$ rational surface in DIII-D discharge #158115 is governed by the nonlinear model.

VI. SUMMARY AND DISCUSSION

This paper investigates the plasma response to an externally generated, static, $n=2$, RMP, whose amplitude is modulated cycloidally at a frequency of 1 Hz, at two rational surfaces located in the pedestal of DIII-D H-mode discharge #158115.[14] The first rational surface is the $m=-8/n=2$ surface, and lies at the top of the pedestal. The second is the $m=-11/n=2$ surface and lies at the bottom of the pedestal. According to the nonlinear, cylindrical, reduced-MHD simulations of Ref. 17, mode penetration at the $-11/2$ surface is responsible for the so-called density pump-out. Moreover, mode penetration at the $-8/2$ surface is hypothesized to be responsible for RMP-induced ELM suppression. This paper examines mode penetration at the $-8/2$ and $-11/2$ surfaces using two asymptotic matching models. The first model is such that the resonant response is linear in nature, and the second is such that the resonant response is nonlinear.

Our linear resonant response model is based on the analysis of Ref. 26, in which the four-field model[58] is used to find all possible linear, two-fluid, drift-MHD, resonant plasma response regimes when a static RMP is applied to a large aspect-ratio tokamak plasma. We deduce that the particular response regime that is appropriate at both the $-8/2$ and $-11/2$ rational surfaces in DIII-D discharge #158115 is the so-called first semi-collisional regime (SCi). Incidentally, it has long been recognized that linear (tearing) layer physics in high-temperature tokamak plasmas is semi-collisional in nature, rather than collisional or collisionless.[34,59,60] Our linear response model does not incorporate the screening effect due to magnetic curvature that was discovered in Ref. 61. However, this effect may be negated by parallel thermal transport.[62] More importantly, the curvature screening effect is a prediction of collisional layer physics, and the true layer physics in tokamak plasmas is semi-collisional. Indeed, Ref. 59 found that, in a semi-collisional layer, the effect of the perturbed bootstrap current is much greater in magnitude than, and opposed to, the effect of magnetic curvature. A much more serious deficiency in our linear layer model emanates from the fact that the layer width is similar to the ion sound radius. Given that the ion and electron temperatures in the pedestal of DIII-D discharge #158115 are almost equal, this implies that the layer width is also similar to the ion gyroradius. Unfortunately, the finite ion gyroradius width is not taken into account in the layer analysis of Ref. 26. Moreover, it is known that, in situations in which the ion gyroradius is similar to, or exceeds, the linear layer width, finite ion orbit width effects can significantly modify the layer response.[59,63]

The linear resonant response model adopted in this paper is augmented by plasma poloidal and toroidal equations of motion that determine how the quasi-linear electromagnetic locking torque that develops at the rational surface, in response to the applied RMP, modifies the local plasma rotation. The equations of motion take plasma perpendicular viscosity, neoclassical poloidal flow-damping, and neoclassical toroidal flow-damping into account. When the equations of motion are combined with the linear resonant response model, a closed set of nonlinear equations is obtained; these equations are solved numerically.

The linear resonant response model is only valid when the width of the RMP-induced magnetic island chain at the rational surface falls below the linear layer width. In the opposite situation, in which the driven island width exceeds the linear layer width, the linear resonant response model must be replaced by a nonlinear resonant response model. It turns out that the appropriate nonlinear resonant response model is, in many ways, simpler than the linear resonant response model, given that it essentially consists of the Rutherford island width evolution equation[33] combined with a no-slip constraint.[30]

The main conclusion of our quasi-linear simulations (i.e., simulations that employ the linear resonant response model), which are described in Sec. V B, is that a linear resonant response model is inapplicable at both the $-8/2$ and $-11/2$ rational surfaces in DIII-D discharge #158115. The problem is that the semi-collisional layer widths at the rational surfaces are so small (a few mm, in both cases) that rotational shielding is not sufficient to reduce the driven magnetic island widths below the layer widths.

Our fully nonlinear simulations (i.e., simulations that employ a nonlinear resonant response model), which are described in Sec. V C, give results that are similar to the experimental results described in Ref. 17. At the $-8/2$ rational surface, driven magnetic reconnection is strongly screened by plasma rotation as long as the resonant component of the radial magnetic field remains below a certain threshold value. However, as soon as the radial field exceeds the threshold value, which is about 6 G, there is a sudden and irreversible breakdown of screening, accompanied by rapid shifts in the local plasma toroidal and poloidal angular velocities. On the other hand, at the $-11/2$ rational surface, the plasma rotation is not large enough to screen driven magnetic reconnection, because the plasma at the bottom of the pedestal is much colder and resistive than that at the top of the pedestal.

There are a number of improvements that could be made to the theory described in this paper. Such improvements include employing a more realistic plasma equilibrium; using a more accurate neoclassical model; calculating the simultaneous responses of multiple resonant surfaces to the applied RMP; including island saturation terms,[64–66]

Published under license by AIP Publishing

the perturbed bootstrap current,[52] and the perturbed ion polarization current,[67] in the Rutherford equation; and taking into account orbit-squeezing effects due to the strong shear in the radial electric field that is typically present in H-mode tokamak pedestals.[68]

ACKNOWLEDGMENTS

This research was funded by the U.S. Department of Energy under Contract No. DE-FG02-04ER-54742. The author would like to thank R. Nazikian, Q. M. Hu, and C. Paz-Soldan for helpful discussions.

APPENDIX A: ELECTRON NEOCLASSICAL EFFECTS

It is helpful to define the electron collisionality at the rational surface[69]

$$\nu_{e*} = 1.13 \times 10^{-3} \left[\frac{|m|}{n\,\hat{r}_s^{3/2}}\right]\left[\frac{R_0^{5/2}\,n_e\,Z_{\rm eff}}{a^{3/2}\,T_e^2}\right]. \tag{A1}$$

Here, $Z_{\rm eff}$ is the effective ion charge number (incidentally, the majority ion charge number is unity), n_e is the equilibrium electron number density at the rational surface, and T_e is the equilibrium electron temperature at the rational surface. Moreover, R_0 is measured in meters, a in meters, n_e in 10^{19} m^{-3}, and T_e in kilo-electron-volts. In accordance with the analysis of Ref. 26, the Coulomb logarithm is assumed to take the value 17 for all plasma species. Now, the fraction of trapped particles at the rational surface, assuming that the plasma there lies in the banana collisionality regime, is[70]

$$f_t = 1.46\left[\hat{r}_s^{1/2}\right]\left[\frac{a^{1/2}}{R_0^{1/2}}\right] - 0.46\left[\hat{r}_s^{3/2}\right]\left[\frac{a^{3/2}}{R_0^{3/2}}\right]. \tag{A2}$$

Let[69,71,72]

$$X = \frac{f_t}{1 + (0.55 - 0.1\,f_t)\,\nu_{e*}^{1/2} + 0.45\,(1 - f_t)\,\nu_{e*}/Z_{\rm eff}^{3/2}} \tag{A3}$$

and

$$F_e = \frac{Z_{\rm eff}}{1 - (1 + 0.36/Z_{\rm eff})\,X + (0.59/Z_{\rm eff})\,X^2 - (0.23/Z_{\rm eff})\,X^3} \times \frac{1 + 1.198\,Z_{\rm eff} + 0.222\,Z_{\rm eff}^2}{1 + 2.966\,Z_{\rm eff} + 0.753\,Z_{\rm eff}^2}. \tag{A4}$$

We can define the effective electron temperature at the rational surface

$$T_{e\rm eff} = \frac{T_e}{F_e^{2/3}}. \tag{A5}$$

This quantity is the electron temperature that gives the correct plasma resistivity, taking into account the effect of impurities and the neoclassical modification of plasma resistivity,[69,71] when plugged into the standard formula $\eta_\parallel = m_e/(n_e\,e^2\,\tau_{ee})$. Here, τ_{ee} is the electron/electron 90° scattering timescale at the rational surface.

APPENDIX B: ION NEOCLASSICAL EFFECTS

It is helpful to define the ion collisionality at the rational surface[69]

$$\nu_{i*} = 9.07 \times 10^{-4} \left[\frac{|m|}{n\,\hat{r}_s^{3/2}}\right]\left[\frac{R_0^{5/2}\,n_e}{a^{3/2}\,T_i^2}\right]. \tag{B1}$$

Here, T_i is the ion temperature at the rational surface, measured in kilo-electron-volts. Let[70,73–75]

$$\hat{K}_{00\rm B} = \alpha + 0.533, \tag{B2}$$

$$\hat{K}_{00\rm P} = 1.77, \tag{B3}$$

$$\hat{K}_{00\rm PS} = \frac{4.25\,\alpha + 3.02}{D}, \tag{B4}$$

$$\hat{K}_{01\rm B} = \alpha + 0.707, \tag{B5}$$

$$\hat{K}_{01\rm P} = 5.32, \tag{B6}$$

$$\hat{K}_{01\rm PS} = \frac{20.13\,\alpha + 12.43}{D}, \tag{B7}$$

$$\hat{K}_{11\rm B} = 2\,\alpha + 1.591, \tag{B8}$$

$$\hat{K}_{11\rm P} = 21.27, \tag{B9}$$

$$\hat{K}_{11\rm PS} = \frac{101.06\,\alpha + 58.65}{D}, \tag{B10}$$

$$D = 2.40\,\alpha^2 + 5.32\,\alpha + 2.225, \tag{B11}$$

$$\alpha = Z_I\left(\frac{Z_{\rm eff} - 1}{Z_I - Z_{\rm eff}}\right). \tag{B12}$$

Here, $Z_i = 1$ and $Z_I = 6$ are the charge numbers of the majority (H^2) and impurity (C^{6+}) ions, respectively. Note that we are making the simplifying (but reasonably accurate) assumptions, that the impurity ion mass is much larger than the majority ion mass that the impurity ion neoclassical viscous force is negligible compared to the friction force acting between the two ion species, and that the two ion species have the same temperature.[70] It follows that:[70,73–75]

$$\hat{K}_{ab} = \frac{\hat{K}_{ab\rm B}}{(1 + 2.92\,\nu_{i*}\,\hat{K}_{ab\rm B}/\hat{K}_{ab\rm P})\left[1 + 2\,\epsilon_s^{3/2}\,\nu_{i*}\,\hat{K}_{ab\rm P}/(3\,\hat{K}_{ab\rm PS})\right]}, \tag{B13}$$

for a, $b = 0$, 1. The normalized ion neoclassical viscosities are written

$$\hat{\mu}_{00i} = g\,\hat{K}_{00}, \tag{B14}$$

$$\hat{\mu}_{01i} = g\left(\frac{5}{2}\,\hat{K}_{00} - \hat{K}_{01}\right), \tag{B15}$$

$$\hat{\mu}_{11i} = g\left(\hat{K}_{11} - 5\,\hat{K}_{01} + \frac{25}{4}\,\hat{K}_{00}\right), \tag{B16}$$

where $g = f_t/(1 - f_t)$.

Let

$$F_i = \left(\frac{q_s}{\epsilon_s}\right)^2 \hat{\mu}_{00i}. \tag{B17}$$

The neoclassical poloidal flow-damping timescale takes the form[70,71]

Published under license by AIP Publishing

$$\tau_\theta = \frac{\tau_{ii}}{F_i}, \tag{B18}$$

where τ_{ii} is the majority-ion/majority-ion 90° scattering timescale at the rational surface.[76] It is helpful to define the effective ion temperature at the rational surface

$$T_{ieff} = \frac{T_i}{F_i^{2/3}}. \tag{B19}$$

This is the temperature at which the neoclassical poloidal flow-damping timescale matches the majority-ion/majority-ion 90° scattering timescale at the rational surface.

According to Ref. 26, the natural frequency of a nonlinear magnetic island chain takes the form

$$\omega_0 = -n\,\omega_E - n\left(1 - \frac{\eta_i\,\lambda_{\theta i}}{1+\eta_i}\right)\omega_{*i}, \tag{B20}$$

where[70,73–75]

$$\lambda_{\theta i} = \frac{\hat{\mu}_{01i}}{\hat{\mu}_{00i} + (\hat{\mu}_{00i}\,\hat{\mu}_{11i} - \hat{\mu}_{01i}^2)/(\sqrt{2} + \alpha - \alpha\,\beta)} \tag{B21}$$

and

$$\beta = \left(\frac{27}{4}\right)^2 \left(\frac{M_i}{M_I}\right)^2 \Big/ \left(\frac{15}{2} + \sqrt{\frac{2\,\alpha\,M_I}{M_i}}\right). \tag{B22}$$

Here, $M_i = 2$ and $M_I = 12$ are the mass numbers of the majority and minority ions, respectively.

APPENDIX C: MODEL PARAMETERS

The hydromagnetic timescale is written as

$$\tau_H = 1.45 \times 10^{-7} \left[\frac{M_i^{1/2}}{n\,s}\right] \left[\frac{R_0\,n_e^{1/2}}{|B_\phi|}\right], \tag{C1}$$

where τ_H is measured in seconds and B_ϕ in tesla. The resistive timescale is written as

$$\tau_R = 2.27 \times 10^{+1} \left[\hat{r}_s^2\right] \left[a^2\,T_{eeff}^{3/2}\right], \tag{C2}$$

where τ_R is measured in seconds. The viscous diffusion timescale is written as

$$\tau_V = \left[\hat{r}_s^2\right] \left[\frac{a^2}{\chi_\perp}\right], \tag{C3}$$

where τ_V is measured in seconds and the perpendicular momentum diffusivity at the rational surface, $\chi_\perp$, is measured in meters squared per second.

The linear layer width is written as

$$\delta_{SC} = 9.36 \times 10^{-4} \left[\frac{\hat{r}_s}{n\,s}\right] \left[\frac{R_0\,a\,n_e^{1/2}\,|n\,\omega_{*e}|^{1/2}}{T_e^{1/2}\,T_{eeff}^{3/4}}\right], \tag{C4}$$

where δ_{SC} is measured in meters. The linear reconnection time is written as

$$\tau_{SC} = 1.06 \times 10^{-2} \left[\frac{\hat{r}_s^2}{n\,s\,|m|}\right] \left[\frac{R_0\,a^2\,n_e^{1/2}\,T_{eeff}^{3/4}\,|n\,\omega_{*e}|^{1/2}}{T_e^{1/2}}\right], \tag{C5}$$

where τ_{SC} is measured in seconds.

The dimensionless plasma viscosity parameter is written as

$$\nu_\mu = 1.06 \times 10^{-2} \left[\frac{\hat{r}_s^2}{n\,s\,|m|}\right] \left[\frac{R_0\,n_e^{1/2}\,T_{eeff}^{3/4}\,\chi_\perp\,|n\,\omega_{*e}|^{1/2}}{T_e^{1/2}}\right]. \tag{C6}$$

The dimensionless plasma poloidal flow-damping parameter is written as

$$\nu_\theta = 2.74 \times 10^{+0} \left[\frac{\hat{r}_s^2}{M_i^{1/2}\,n\,s\,|m|}\right] \left[\frac{R_0\,a^2\,n_e^{3/2}\,T_{eeff}^{3/4}\,|n\,\omega_{*e}|^{1/2}}{T_e^{1/2}\,T_{ieff}^{3/2}}\right]. \tag{C7}$$

The dimensionless locking parameter, L, is written as

$$L = 1.61 \times 10^{-5} \left[\frac{\hat{r}_s^8}{M_i\,n^4\,s^4\,|m|}\right] \left[\frac{R_0^4\,a^4\,n_e^2\,B_\phi^2\,|n\,\omega_{*e}|^3}{T_e^{3/2}\,T_{eeff}^{3/2}}\right]. \tag{C8}$$

The normalized natural frequency is written as

$$\hat{\omega}_0 = 1.06 \times 10^{+1} \left[\frac{\hat{r}_s^2}{n\,s\,|m|}\right] \left[\frac{R_0\,a^2\,n_e^{1/2}\,T_{eeff}^{3/4}\,|n\,\omega_{*e}|^{1/2}}{T_e^{1/2}}\right] \omega_0, \tag{C9}$$

where ω_0 is measured in kilo-radians per second. The normalized radial magnetic field is written as

$$b_f = 1.83 \times 10^{+3} \left[\frac{n\,s}{\hat{r}_s}\right] \left[\frac{T_e\,T_{eeff}^{3/2}}{R_0\,a\,n_e\,|B_\phi|\,|n\,\omega_{*e}|}\right] b_v, \tag{C10}$$

where the vacuum radial magnetic field at the rational surface, b_v, is measured in gauss.

REFERENCES

[1] F. Wagner, G. Becker, K. Behringer, D. Campbell, A. Eberhagen, W. Engelhardt, G. Fussmann, O. Gehre, J. Gernhardt, G. V. Gierke *et al.*, Phys. Rev. Lett. **49**, 1408 (1982).
[2] H. Zohm, Plasma Phys. Controlled Fusion **38**, 105 (1996).
[3] N. Den Harden, S. Brezinsek, T. Pütterich, N. Fedorczak, G. F. Matthews, A. Meigs, M. F. Stamp, M. C. M. van de Sanden, G. J. Van Rooij, and JET Contributors, Nucl. Fusion **56**, 026014 (2016).
[4] A. Loarte, G. Saibene, R. Sartori, M. Bécoulet, L. Horton, T. Eich, A. Herrmann, M. Laux, G. Matthews, S. Jachmich *et al.*, J. Nucl. Mater. **313-316**, 962 (2003).
[5] T. E. Evans, R. A. Moyer, J. G. Watkins, P. R. Thomas, T. H. Osborne, J. A. Boedo, M. E. Fenstermacher, K. H. Finken, R. J. Groebner, M. Groth *et al.*, Phys. Rev. Lett. **92**, 235003 (2004).
[6] Y. Liang, H. R. Koslowski, P. R. Thomas, E. Nardon, B. Alper, P. Andrew, Y. Andrew, G. Arnoux, Y. Baranov, M. Bécoulet *et al.*, Phys. Rev. Lett. **98**, 265004 (2007).
[7] W. Suttrop, T. Eich, J. C. Fuchs, S. Günter, A. Janzer, A. Herrmann, A. Kallenbach, P. T. Lang, T. Lunt, M. Maraschek *et al.*, Phys. Rev. Lett. **106**, 225004 (2011).
[8] Y. M. Jeon, J.-K. Park, S. W. Yoon, W. H. Ko, S. G. Lee, K. D. Lee, G. S. Yun, Y. U. Nam, W. C. Kim, J.-G. Kwak, K. S. Lee, H. K. Kim, H. L. Yang *et al.*, Phys. Rev. Lett. **109**, 035004 (2012).
[9] A. Kirk, I. T. Chapman, Y. Liu, P. Cahyna, P. Denner, G. Fishpool, C. J. Ham, J. R. Harrison, Y. Liang, E. Nardon, S. Saarelma, R. Scannell, A. J. Thornton, and MAST Team, Nucl. Fusion **53**, 043007 (2013).

Published under license by AIP Publishing

[10]T. Sun, Y. Liang, Y. Q. Liu, S. Gu, X. Yang, W. Guo, T. Shi, M. Jia, L. Wang, B. Lyu *et al.*, Phys. Rev. Lett. **117**, 115001 (2016).
[11]J. W. Connor, R. J. Hastie, H. R. Wilson, and R. L. Miller, Phys. Plasmas **5**, 2687 (1998).
[12]M. E. Fenstermacher, T. E. Evans, T. H. Osborne, M. J. Schaffer, M. P. Aldan, J. S. deGrassie, P. Gohil, I. Joseph, R. A. Moyer, P. B. Snyder, R. J. Groebner, M. Jakubowski, A. W. Leonard, O. Schmitz, and DIII-D Team, Phys. Plasmas **15**, 056122 (2008).
[13]M. Bécoulet, F. Orain, P. Maget, N. Mellet, X. Garbet, E. Nardon, G. T. A. Huijsmans, T. Casper, A. Loarte, P. Cahyna, A. Smolyakov *et al.*, Nucl. Fusion **52**, 054003 (2012).
[14]R. Nazikian, C. Paz-Soldan, J. D. Callen, J. S. deGrassie, D. Eldon, T. E. Evans, N. M. Ferraro, B. A. Grierson, R. J. Groebner, S. R. Haskey *et al.*, Phys. Rev. Lett. **114**, 105002 (2015).
[15]F. Orain, M. Hoelzl, F. Mink, M. Willensdorfer, M. Bécoulet, M. Dunne, S. Günter, G. T. A. Huijsmans, K. Lackner, S. Pamela *et al.*, Phys. Plasmas **26**, 042503 (2019).
[16]S. K. Kim, S. Pamela, O. Kwon, M. Becoulét, G. T. A. Huijsmans, Y. In, M. Hoelzl, J. H. Lee, M. Kim, G. Y. Park *et al.*, Nucl. Fusion **60**, 026009 (2020).
[17]Q. M. Hu, R. Nazikian, B. A. Grierson, N. C. Logan, J.-K. Park, C. Paz-Soldan, and Q. Yu, Phys. Plasmas **26**, 120702 (2019).
[18]Q. Yu, S. Günter, and B. D. Scott, Phys. Plasmas **10**, 797 (2003).
[19]Q. Yu, Nucl. Fusion **50**, 025014 (2010).
[20]Q. Yu and S. Günter, Nucl. Fusion **51**, 073030 (2011).
[21]C. Paz-Solden, R. Nazikian, S. R. Haskey, N. C. Logan, E. J. Strait, N. M. Ferraro, J. M. Hanson, J. D. King, M. J. Lanctot, R. A. Moyer *et al.*, Phys. Rev. Lett. **114**, 105001 (2015).
[22]C. Paz-Solden, N. C. Logan, S. R. Haskey, R. Nazikian, E. J. Strait, X. Chen, N. M. Ferraro, J. D. King, B. C. Lyons, and J.-K. Park, Nucl. Fusion **56**, 056001 (2016).
[23]K. Harafuji, T. Hayashi, and J. Sato, J. Comput. Phys. **81**, 169 (1989).
[24]J.-K. Park, A. Boozer, and A. H. Glasser, Phys. Plasmas **14**, 052110 (2007).
[25]R. Fitzpatrick and F. L. Waelbroeck, Phys. Plasmas **12**, 022307 (2005).
[26]A. J. Cole and R. Fitzpatrick, Phys. Plasmas **13**, 032503 (2006).
[27]R. Fitzpatrick, Phys. Plasmas **21**, 092513 (2014).
[28]R. Fitzpatrick, Phys. Plasmas **25**, 082513 (2018).
[29]R. Fitzpatrick, Phys. Plasmas **25**, 112505 (2018).
[30]R. Fitzpatrick, Nucl. Fusion **33**, 1049 (1993).
[31]H. P. Furth, J. Killeen, and M. N. Rosenbluth, Phys. Fluids **6**, 459 (1963).
[32]F. L. Waelbroeck, Nucl. Fusion **49**, 104025 (2009).
[33]P. H. Rutherford, Phys. Fluids **16**, 1903 (1973).
[34]J. F. Drake and Y. C. Lee, Phys. Fluids **20**, 1341 (1977).
[35]F. L. Waelbroeck, Phys. Plasmas **10**, 4040 (2003).
[36]R. J. Hawryluk, "An empirical approach to plasma transport," in *Physics of Plasma Close to Thermonuclear Conditions* (Commission of the European Communities, Brussels, 1980), Vol. 1.
[37]R. Fitzpatrick, Phys. Plasmas **5**, 3325 (1998).
[38]P. H. Rutherford, "Basic physical processes of toroidal fusion plasmas," in *Proceedings of Course and Workshop, Varenna* (Commission of the European Communities, Brussels, 1985), Vol. 2, p. 531.
[39]A. I. Smolyakov, Plasma Phys. Controlled Fusion **35**, 657 (1993).
[40]A. I. Smolyakov, A. Hirose, E. Lazzaro, G. B. Re, and J. D. Callen, Phys. Plasmas **2**, 1581 (1995).
[41]R. Fitzpatrick, R. J. Hastie, T. J. Martin, and C. M. Roach, Nucl. Fusion **33**, 1533 (1993).
[42]R. Fitzpatrick, Phys. Plasmas **24**, 072506 (2017).
[43]G. Berge, L. K. Sandal, and J. A. Wesson, Phys. Scr. **40**, 173 (1989).
[44]S. P. Hirshman, Nucl. Fusion **18**, 917 (1978).
[45]J. D. Callen, A. J. Cole, and C. C. Hegna, Nucl. Fusion **49**, 085021 (2009).
[46]T. H. Stix, Phys. Fluids **16**, 1260 (1973).
[47]K. Shaing, Phys. Plasmas **10**, 1443 (2003).
[48]A. J. Cole, C. C. Hegna, and J. D. Callen, Phys. Plasmas **15**, 056102 (2008).
[49]B. E. Chapman, R. Fitzpatrick, D. Craig, P. Martin, and G. Spizza, Phys. Plasmas **11**, 2156 (2004).
[50]*Handbook of Mathematical Functions with Formulas, Graphs, and Mathematical Tables*, edited by M. Abramowitz and I. A. Stegun (Dover, New York, NY, 1965), Chap. 9.
[51]I. S. Gradshteyn and I. M. Ryzhik, *Table of Integrals, Series, and Products, Corrected and Enlarged Edition* (Academic Press, New York, NY, 1980).
[52]R. Fitzpatrick, Phys. Plasmas **2**, 825 (1995).
[53]C. Paz-Soldan, private communication (2019).
[54]R. Nazikian, C. C. Petty, A. Bortolon, X. Chen, D. Eldon, T. E. Evans, B. A. Grierson, N. M. Ferraro, S. R. Haskey, M. Knolker *et al.*, Nucl. Fusion **58**, 106010 (2018).
[55]C. Paz-Soldan, R. Nazikian, L. Cui, B. C. Lyons, D. M. Orlov, A. Kirk, N. C. Logan, T. H. Osborne, W. Suttrop, and D. B. Weisberg, Nucl. Fusion **59**, 056012 (2019).
[56]R. J. La Haye, C. C. Petty, E. J. Strait, F. L. Waelbroeck, and H. R. Wilson, Phys. Plasmas **10**, 3644 (2003).
[57]P. Buratti, E. Alessi, M. Baruzzo, A. Casolari, E. Giovannozzi, C. Giroud, N. Hawkes, S. Menmuir, G. Pucella, and JET Contributors, Nucl. Fusion **56**, 076004 (2016).
[58]R. D. Hazeltine, M. Kotschenreuther, and P. J. Morrison, Phys. Fluids **28**, 2466 (1985).
[59]R. Fitzpatrick, Phys. Fluids B **1**, 2381 (1989).
[60]J. W. Connor, R. J. Hastie, and P. Helander, J. Plasma Phys. **83**, 905830608 (2017).
[61]Y. Q. Liu, A. Kirk, Y. Sun, P. Cahyna, I. T. Chapman, P. Denner, G. Fishpool, A. M. Garofalo, J. R. Harrison, E. Nardon, and MAST Team, Phys. Plasmas **19**, 072509 (2012).
[62]X. Bai, Y. Q. Liu, and Z. Gao, Phys. Plasmas **24**, 102505 (2017).
[63]S. C. Cowley, R. M. Kulsrud, and T. S. Hahm, Phys. Fluids **29**, 3230 (1986).
[64]A. Thyagaraja, Phys. Fluids **24**, 1716 (1981).
[65]D. F. Escande and M. Ottaviani, Phys. Lett. A **323**, 278 (2004).
[66]R. J. Hastie, F. Militello, and F. Porcelli, Phys. Rev. Lett. **95**, 065001 (2005).
[67]R. Fitzpatrick, Plasma Phys. Controlled Fusion **54**, 094002 (2012).
[68]F. L. Hinton and Y. B. Kim, Phys. Plasmas **2**, 159 (1995).
[69]O. Sauter, C. Angioni, and Y. R. Lin-Liu, Phys. Plasmas **6**, 2834 (1999).
[70]Y. B. Kim, P. H. Diamond, and R. J. Groebner, Phys. Fluids B **3**, 2050 (1991).
[71]S. P. Hirshman, Phys. Fluids **21**, 1295 (1978).
[72]M. C. Zarnstorff, M. G. Bell, M. Bitter, R. J. Goldston, B. Grek, R. J. Hawryluk, K. Hill, D. Johnson, D. McCune, H. Park, A. Ramsey, G. Taylor, and R. Wieland, Phys. Fluids B **2**, 1852 (1990).
[73]S. P. Hirshman and D. J. Sigmar, Nucl. Fusion **21**, 1079 (1981).
[74]Y. B. Kim, P. H. Diamond, and J. Groebner, Phys. Fluids B **4**, 2996 (1992).
[75]J. D. Callen, "Viscous forces due to collisional parallel stresses for extended MHD codes," Report No. UW-CPTC 09-CR (2010).
[76]R. Fitzpatrick, *Plasma Physics: An Introduction* (Taylor & Francis, Abingdon, UK, 2014).

Published under license by AIP Publishing